GTI PROJECT # 15340

OXIDATION OF DRY HYDROCARBONS AT HIGH-POWER DENSITY ANODES

Final Report

October 1, 2002 to December 31, 2003

Submitted By:

Gas Technology Institute
1700 S. Mount Prospect Rd.
Des Plaines, Illinois 60018
www.gastechnology.org

Prepared by:

K. Krist, O. Spaldon-Stewart, R. Remick

March 2004

DOE Award Number: DE-FC26-02NT41573

DISCLAIMER

This report was prepared as an account of work sponsored by an agency of the United States Government. Neither the United States Government nor any agency thereof, nor any of their employees, makes any warranty, express or implied, or assumes any legal liability or responsibility for the accuracy, completeness, or usefulness of any information, apparatus, product, or process disclosed, or represents that its use would not infringe privately owned rights. Reference herein to any specific commercial product, process, or service by trade name, trademark, manufacturer, or otherwise does not necessarily constitute or imply its endorsement, recommendation, or favoring by the United States Government or any agency thereof. The views and opinions of authors expressed herein do not necessarily state or reflect those of the United States Government or any agency thereof.

ABSTRACT

This work builds upon discoveries by the University of Pennsylvania and others pertaining to the oxidation of dry hydrocarbon fuels in high temperature solid oxide fuel cells. The work reported here was restricted primarily to dry methane and confirms that YSZ-based cells, having ceria in the anode as a catalyst and copper in the anode as a current collector, can operate on dry methane for extended periods. Thirty-three lab-scale cells of various designs were fabricated and operated under a variety of conditions. The longest-lived cell gave stable performance on dry methane at 800°C for over 305 hours. Only slight carbon deposition was noted at the completion of the test. A corresponding nickel/YSZ-based anode would have lasted for less than an hour under these test conditions (which included open circuit potential measurements) before carbon fouling essentially destroyed the cell. The best performing cell achieved 112 mW/cm^2 on dry methane at 800°C.

Several problems were encountered with carbon fouling and declining open circuit voltages in many of the test cells after switching from operation on hydrogen to dry methane. Although not rigorously confirmed by experimentation, the results suggested that air infiltration through less than perfect perimeter seals or pinholes in the electrolytes, or both gave rise to conditions that caused the carbon fouling and OCV decline. Small amounts of air reacting with methane in a partial oxidation reaction could produce carbon monoxide that, in turn, would deposit the carbon. If this mechanism is confirmed, it implies that near perfect hardware is required for extended operation. Some evidence was also found for the formation of electrical shorts, probably from carbon deposits bridging the electrolyte.

Work with odorized methane and with methane containing 100-ppm hydrogen sulfide confirmed that copper is stable at 800°C in dry hydrocarbon fuels in the presence of sulfur. In a number of cases, but not exclusively, the performance life on dry methane with sulfur compounds was much longer than with dry methane alone. The effect of sulfur compounds in these cases appeared to correlate with inhibition of carbon deposition. Mixed results were obtained for the effect of the sulfur compounds on power density.

Progress also was made in understanding the mechanisms involved in direct utilization of dry natural gas. Evidence was developed for three possible mechanisms for dry methane utilization in addition to the usually cited mechanism - direct oxidation of methane by oxygen anions. Further work is required at a fundamental level before the knowledge gained here can be translated into higher levels of performance.

TABLE OF CONTENTS

LIST OF GRAPHICAL MATERIALS

INTRODUCTION

Background

Traditionally, high-temperature fuel processing systems, employ steam-to-carbon ratios of >3:1 in order to prevent carbon deposition when operating on hydrocarbon fuels.

SOFC systems may provide this steam by recycling the anode outlet gas. For example, some tubular SOFC systems recycle spent fuel - containing steam, CO_2 and residual H_2 - to a pre-reformer. Indirect internal reforming completes the processing of the pre-reformed fuel before it enters the fuel compartment. This recycle of anode exhaust provides sufficient steam to prevent carbon formation; externally supplied steam is only needed for start up. The supply and treatment issues associated with an external water source are avoided, although the fuel is also diluted – decreasing the available Nernst potential somewhat.

Water management may differ for other reforming approaches. If the fuel is not pre-reformed and/or the anode outlet is not recycled, the tendency for carbon deposition may increase because of decreased H_2 content, increased higher hydrocarbon content, and decreased oxygen activity at the anode inlet. In these cases, co-feeding external steam and fuel may be necessary.

To simplify water management and to avoid sintering associated with high steam levels in the anode, the research community is seeking to reduce steam-to-carbon ratios (Singhal and Kendall, 2003). These efforts focus on reducing steam-to-carbon ratios to their thermodynamic limit (~1.5-2.0 for methane reforming).

This project focused on an extension of this approach, which the research community is also investigating – the possibility of operating with little or no steam present. Under these conditions, which can occur at start-up or at low fuel utilizations - direct utilization of the dry hydrocarbon fuel would occur. Such systems would conceivably:

- Not require a pre-reformer normally needed to convert higher hydrocarbons to methane and provide sufficient H_2 to prevent overcooling at the anode inlet
- Avoid the need for anode recycle
- Operate on as-received hydrocarbon fuels, if the anodes were also sulfur tolerant – eliminating the need for fuel processing and contaminant removal upstream of the stack.

Thermodynamics strongly allows carbon deposition by dry hydrocarbon fuels at SOFC operating temperatures. Only kinetic approaches are available to inhibit carbon deposition.

The research community has pursued three types of anodes for directly utilizing dry hydrocarbon fuel.

Conductive Ceramic Anodes

Various groups are using electrically conductive ceramic anodes to operate on dry hydrocarbon fuels (Singhal and Kendall, 2003). The materials investigated include substituted $LaCrO_3$, $SrTiO_3$, $LaMnO_3$, and CeO_2. Thick (2mm) electrolyte-supported, button cells involving these materials have produced maximum power densities of up to ~0.2 W/cm^2 with minimal coking - at 900C on humidified CH_4 at low gas utilizations (Tao and Irvine, 2004).

The technical challenges for this continuing research area include:

- Relatively low electronically conductivity – < ~1-20 S/cm at the low pO_2 in the fuel compartment (Remick, et. al., 1988; Singhal, et. al., 1986; Marina, et. al., 2002).
- Low thermal conductivity - typically ~2 orders below those of conductive metals such as Cu and Ni; this limits the dissipation of heat generated in a fuel cell stack.
- Low exchange current densities for direct utilization of hydrocarbon fuel, resulting in low power densities under practical fuel utilizations, cell areas, and operating voltages.
- Lack of material stability during fabrication or operation caused by, e.g., multiple phases, uncontrolled sintering, and chemical interaction with other cell materials (Stevenson, et. al., 2003; Marina, et. al., 2002; Tao and Irvine, 2004; Pudmich, et. al., 2000).

Ni-Containing Cermet Anodes, Operating At Low Temperature

Northwestern University (Murray, et. al., 1999) has operated dry hydrocarbon fuels with Ni-ceria cermet anodes. Catalysis of hydrocarbon cracking by Ni-containing systems is minimized below 700°C for some hydrocarbons. A mixed potential results due to the carbon/oxygen redox couple and the H_2/O_2 redox couple. Carbon formation is still favored the Boudouard reaction as the temperature decreases, but the effect is mitigated by slower kinetics. Operation at ~500-650C with CH_4 minimizes contributions from these processes.

However, carbon deposition increases as the hydrocarbon chain length increases. Northwestern U. results suggest that progressively lower temperatures are required to oxidize ethane, propane, etc. This limits the applicability of this approach to natural gas, which contains 5-10% of higher hydrocarbons, and also to other gaseous and liquid hydrocarbon fuels.

Ni-Containing Cermet Anodes, Operating At High Temperature

Above ~700°C, even though carbon should quickly foul the cell, NWU has reported that only trace amounts of carbon form if a Ni/YSZ anode cell, operating on dry CH_4, maintains a high current density (Liu and Barnett, 2003). However, open circuit conditions cause significant carbon deposition. Under load, H_2O, CO_2 and/or oxygen anions produced by the electrochemistry appear to convert carbon as it forms so that it does not build up. This suggests that relatively high oxygen activity in the region of the anode near the electrolyte may limit carbon formation.

Cu-Containing Anodes

The SECA Core project investigated Cu-containing anodes. The research was based on previous results from U-Penn, U-Utah, Material and Systems Research, Inc. (MSRI) and the Gas Technology Institute (GTI):

- University of Pennsylvania (U-Penn) had shown that small, laboratory cells containing Cu- and ceria-impregnated, porous, YSZ anodes could operate on hydrocarbons for long periods with only trace amounts of carbon deposition (Park et. al., 1999). The anode could kinetically reduce carbon formation up to 800 C and with higher hydrocarbons than CH_4. The anode also improved sulfur tolerance. However, the power densities were low.

  A mechanism for dry hydrocarbon utilization in these cells was proposed involving oxidation of the hydrocarbon by oxygen anions transported across the cell electrolyte.

- U-Utah and MSRI had developed a high power density, nickel-cermet anode employing an active inter-layer for operation on H_2 and reformate - that was, however, not sulfur tolerant and required high steam levels to avoid carbon.
- GTI had developed intellectual property on sulfur-tolerant, copper anodes for carbonate fuel cells.

Original Plan

The proposal outlined several approaches for increasing the power-density of Cu-based anodes when utilizing as-received hydrocarbon fuels (i.e., near dry and containing sulfur). The goal was to develop an anode that would tolerate sulfur and perform better electrochemically on essentially dry hydrocarbon fuels without forming carbon.

To improve catalytic activity and power density, GTI proposed to introduce a thin, active inter-layer between a thick, anode support and a thin electrolyte. This interlayer contained micron and/or nano-crystalline Cu/Ni, Cu/NiAl, NiAl and other compositions distributed uniformly or in selected regions. Although the more catalytic constituents, e.g., Ni, form carbon and do not tolerate sulfur, these negative effects were diminished because (1) the constituents were only present in a thin interlayer, (2) under load, the relatively high inter-layer oxygen activity might reverse sulfur or carbon poisoning, and (3) the active constituents could be mixed with other less vulnerable constituents. Cu/ceria/YSZ compositions provided for sulfur tolerance and a low steam-to-carbon ratio in the support portion of the anode.

The melting points of Cu, Cu_2O, and CuO are 1083^{o}C, 1235^{o}C, and 1326^{o}C, respectively. Sintering YSZ normally requires temperatures >1400^{o}C. A co-sintering process would therefore melt any Cu present. U-Penn had previously avoided Cu melting by pre-sintering a porous/dense YSZ bi-layer tape and then impregnating the porous layer with ceria and copper salts to form the anode. However, this *dual tape-casting* method did not easily provide for the very thin, high three-phase boundary length, interlayer region that is critical for increasing power density or for the very thin electrolyte needed to reduce ohmic loss at 700 – 800^{o}C.

GTI proposed new methods to avoid Cu melting. Each involved:

- Fabricating a thin, (~20μ each) inter-layer and electrolyte sequentially on an anode support. In some cases, bisquing was used to remove binder, provide green strength, and matched shrinkage profiles.
- Spray coating the thin layers to minimize binder and stresses due to thermal expansion mismatch
- Applying a cathode and sintering either before impregnation of Cu_xO or so as to avoid Cu_xO melting
- Reducing Cu_xO in-cell prior to testing.

Method 1: Wet-Impregnated, Tape Cast Support

The proposed method involved initially tape casting a thick YSZ anode support with pore formers. μm -size powders were to be used to minimize binder content and shrinkage. The support would then be bisqued at ~1000^{o}C and spray coated to form an interlayer consisting of premixed, combinations of selected powders. The inter-layer particle size was to be varied from μm- to nm-crystalline to optimize structure. A μm particle-size electrolyte would then be

sprayed onto the anode interlayer and the porous, YSZ, anode support/anode interlayer/YSZ electrolyte would be sintered at 1400-1550°C. Applying the cathode and sintering it at 1250°C and conducting multiple impregnations and calcinations of the anode with Cu/Ce nitrates would complete fabrication.

Method 2: Dye-Pressed Support Structure

This method involved dry powder pressing an anode support from μm- or nm-crystalline combinations of Cu_xO and CeO_2 powders and nm-crystalline YSZ powders mixed with pore formers such as graphite flake. Dry pressing would reduce the binder in nm-crystalline samples and avoid the need for anode impregnation. The anode support would then be bisqued and spray coated with nm-crystalline material to form an active inter-layer, consisting of premixed, combinations of selected powders. Spray coating a nm-crystalline YSZ electrolyte onto the inter-layer, applying a nm-crystalline cathode, and sintering the complete cell below the Cu_xO melting point would complete fabrication.

Method 3: Tape-Cast Support Structure Using Cermet Powders

This method involved tape casting a complete, porous, anode support from μm-sized Cu_xO/YSZ cermet and ceria powders or μm -sized Cu_xO/YSZ/ceria cermet powders, each mixed with graphite flake and other pore formers. Despite sintering above the melting point of Cu_xO, the cermet powder might retain Cu_xO. The active interlayer and electrolyte would be applied similar to the previous methods and the resulting structure would be sintered at 1400-1550°C. Applying and sintering the cathode at 1250°C would complete fabrication.

Plan Modification

The project was not able to focus much on the fabrication of anode interlayer cells for the reasons cited below. The findings that were obtained may, nevertheless, be useful for future research. Project changes included:

- The basic mechanism of direct utilization was not well understood. Some evidence suggested that oxygen anions in the ceria directly oxidized dry hydrocarbon fuel. However, water vapor produced during the electrochemical reaction also could reform the hydrocarbon. Trace amounts of O_2 or water vapor leaking through the seals, or electrolyte pinholes, or present as contamination of the fuel could convert the hydrocarbon. Since the mechanism could affect interpretation of the results, GTI evaluated the reaction pathway.
- The initially proposed fabrication methods proved to be difficult to implement. However, GTI developed closely related methods as discussed in the Experimental section.
- Fabrication of initial baseline ~3-cm^2 cells that did not contain the active inter-layer presented a number of issues. These included:
    1. Less than perfect integrity of the thin (10μm) electrolyte needed for increased power density
    2. Inadequate seals
    3. Less than desired electrode pore size and porosity
    4. Slow, uneven impregnation due to the small pore size and low porosity in the anode

5. Inadequate cell mechanical strength that led to worries about cracking in various tests
6. Cell warping during sintering and cathode application
7. A contact resistance associated with the cell current collecting screens and/or current leads.

- Additional issues related to the test stand and operating conditions:
  1. The electrical resistance associated with the test set-up was not very reproducible
  2. Temporary power outages and line voltage fluctuations caused un-planned thermal cycles
  3. The test configuration may not have provided sufficient support for the cell.
- Some or all of these problems may have contributed to carbon formation and compromised cell performance. To resolve the cell fabrication, testing, and carbon deposition issues, GTI set up a task to interact with U-Penn.
- In addition to "standard" thin electrolyte cells having an electrolyte thickness of ~13 μm and anode thickness of ~600 μm, cells with electrolyte thickness of ~60 – 100 μm and anode thickness of ~200-400 μm were fabricated to eliminate the possibility that imperfections were shorting or otherwise compromising the cell.
- The cell and test stand issues caused the project to focus on H_2, methane, and natural gas fuels. Higher hydrocarbon fuels were not studied. However, the focus on CH_4 and natural gas complemented the literature emphasis on higher hydrocarbons.

EXECUTIVE SUMMARY

Objective

The University of Pennsylvania (U-Penn) has previously reported dry hydrocarbon oxidation without carbon fouling up to 800°C on porous YSZ anodes impregnated with copper (Cu) and ceria. The cells also exhibited an improved level of sulfur tolerance. The purpose of the GTI project was to develop these systems further to increase power density and operating lifetime. The approach was to introduce a catalytic interlayer (e.g. Ni/YSZ) between Cu/ceria/YSZ anode support and the electrolyte. During this project, Northwestern University (NWU) operated anode-supported Ni/YSZ cells on methane and natural gas in the presence of only 3% water vapor at 600 to 800°C. The NWU cells could operate at high power density but experienced carbon fouling at open circuit.

Cell Selection

U-Penn used 0.33-cm^2 cells cemented to the end of a ceramic tube. Gold (Au) wire current collectors were glued to the anode using an Au paste. Platinum (Pt) or silver (Ag) wire current collectors were glued to the cathode using Pt or Ag paste. This arrangement provides good electrical contact in small cells, but is not conducive to scale up. GTI used a lab-scale cell design that has been proven to predict the performance in large fuel cells. The GTI design used a fine mesh Cu screen backed by a perforated Cu plate as a current collector on the anode side and a fine-mesh Ag screen and perforated Ag plate as a current collector on the cathode side. No paste or ink was used to bond the current collector to the electrode. The GTI cells have a relationship between interfacial resistance and holding force similar to that found in most fuel cell stacks.

The GTI design sandwiched the cell between ceramic tubes using compliant seals. The edges of the porous anode were not sealed and fuel gas could diffuse out of the cell. Cathode-side seals between the ceramic tube and the dense electrolyte prevented air from diffusing outside of the cell. A flat-ring mica gasket was used as a compliant seal. Thin layers of tape cast talc were placed between the mica gasket and the ceramic tube and between the mica and the fuel cell. The talc filled in surface imperfections to make an excellent seal that, because of the soft nature of the talc, can thermal cycle without stressing the cell. However, it cannot provide the excellent gas-tight seal of dense cement. During the latter half of the project, a zirconia cement was used on the cathode side to prevent fuel from diffusing into the cathode. This cement hardened during heat up so that GTI cells using cement seals were not able to thermal cycle without cracking.

Principal Findings

Thirty-three lab-scale cells were fabricated and operated under a variety of conditions. Fuels included dry H_2, humidified H_2, dry CH_4, humidified CH_4, N_2-diluted CH_4, CH_4 with sulfur compounds, N_2 and CH_4 with sulfur compounds, and as-received dry natural gas. The principal findings were:

- Baseline performance data at 700 and 800C suggested that carbon deposition varies strongly with factors as electrolyte integrity, seal integrity, the effect of sulfur compounds, temperature, anode structure, and hardware design.
- Carbon fouling plagued some tests, although not in a consistent manner. Carbon fouling is defined here as the buildup of carbon so as to disrupt the physical structure of the cell.

Some cells operated for several hundred hours on dry methane fuel at 800°C without fouling. Others died in less than twenty-four hours.

- The results suggest that the infiltration of oxidant (air) and/or water vapor through the seals or the electrolyte caused partial oxidation or reforming of CH_4 in the interior of the anode, producing carbon monoxide that then deposited carbon in the anode. The more air infiltration, the shorter the time-to-failure. In general, thicker-electrolyte cells appeared to exhibit higher OCVs than thin-electrolyte cells and had longer time-to-failure.
- The addition of sulfur compounds to dry CH_4 appeared to inhibit carbon deposition and extend cell life. Tests conducted with CH_4 odorized with a combination of organic sulfur species and carbonyl sulfide up to 75 ppm total sulfur indicated complete sulfur tolerance. In all experiments, no change in performance was observed. However, when CH_4 containing 100 ppm H_2S was used, the performance decayed in some tests, but not others.
- OCV declines with time often observed after switching fuel from H_2 to dry CH_4 may be due to the formation of carbon bridges across the electrolyte that short the cell or to other effects of carbon deposition such as increased air infiltration through compromised seals. The OCV decline is accompanied by electrochemical performance decline under load.
- Although little work was performed because of the carbon deposition issue, the project showed that the originally proposed Ni interlayer cells could be fabricated and produced power densities, cell life, and sulfur tolerance comparable to cells not containing an interlayer.
- Mechanisms were identified based on internal reforming, partial oxidation, and reduction of ceria in the anode as alternative routes for direct utilization of CH_4. The mechanism involving ceria reduction leads to an interpretation of how and where carbon deposits in comparison with previous explanations involving only gas phase cracking. The mechanism also shows how carbon deposition may be self-limiting at 700-750C.

General Conclusions

As a consequence of using sintered porous YSZ as the main structural support, the cells tend to be fragile. The standard approaches to increasing performance that was used in this project (increasing anode porosity, decreasing anode thickness, decreasing electrolyte thickness and adding an anode/electrolyte interlayer) work against component structural integrity. While the program confirmed that Cu-ceria impregnated cells are active for directly utilizing dry CH_4, the best performance achieved was below that needed for commercialization. Sulfur tolerance was confirmed at levels well above those generally found in odorized natural gas.

The results of this project enhance, rather than diminish, the promise of these cells. The elimination of virtually all fuel processing hardware from the fuel cell system might offset the increased costs of a lower output from the fuel cell stack. However, these cells clearly have unique challenges with respect to materials selection and component fabrication that need to be addressed by additional research.

EXPERIMENTAL

Cell Fabrication

U-Penn Method

The U-Penn anode uses a porous YSZ skeleton, impregnated with Cu and Ce oxide, as the supporting structure (Gorte, et. al., 2000). A thin YSZ tape is cast will become the ~25 – 80-µm thick electrolyte layer when sintered. After drying, a layer of YSZ mixed with pore former is cast on top of the first tape. This second layer is also dried in air. The two-layer tape is air sintered at ~1550°C. During firing, the pore former in the second tape burns off, leaving a porous structure, while the YSZ in the first tape forms a dense electrolyte layer that bonds tightly to the porous layer. U-Penn (Gorte, et. al., 2000) and Corbin and Apté (1999) have suggested that the relative shrinkage of porous and dense layers do not change during sintering, allowing co-sintering without warping or cracking.

After sintering, LSM + YSZ is applied to the electrolyte and sintered at ~1200°C. The three-layer structure is flipped, turning up the porous YSZ layer. The porous layer is impregnated with aqueous Ce (IV) nitrate and dried. The structure is then heated to several hundred degrees to decompose the nitrate leaving behind CeO_2 in the pores. The impregnation is repeated until the weight of CeO_2 is 10%. The porous structure is then impregnated with an aqueous Cu (II) nitrate and again heated to drive off the water and decompose the nitrate. This step is repeated until the loading of Cu (II) oxide is 20 wt %. When the cell is assembled in a clamping fixture and fuel gases passed over the porous anode, the copper (II) oxide in the pores will reduce to Cu and act as the current collector.

Baseline GTI-Fabricated Cell

Table I summarizes a baseline procedure – similar to that of U-Penn - used to fabricate most of the GTI cells.

Table I: Baseline GTI Cell Fabrication

Method	Comments
1. Dual tape cast, dense YSZ electrolyte/porous YSZ anode bi-layer, followed by painted LSM + YSZ cathode and impregnation of the anode with Cu and ceria salts.	**Main fabrication method. Porous anode support tape was cast over electrolyte tape. Used for both "thin" and "thick" electrolyte cells. Replaced proposed spray-coating methods for which substrate pore size was too high. Tape casting was entirely water based. Methocel K35-LV was used as a binder.** **30 wt% 43-µm graphite flake pore formers were used for most of the anodes. This increased both geometric porosity and median pore size to ~55% and ~1.4 µm, respectively, as measured by Hg intrusion porosimetry. A combination of graphite powder and PMMA was used later to increase these values further. Pore formers were not used in the cathode.** **Samples were sintered between two refractory-fiber boards, Zircar ZAL-15 to creep flatten, and slowly heated first to 550°C, then 1550°C.** **The cells always had LSM/8YSZ cathode inter-layers and usually had an additional LSM layer. In thin-anode cells (see below), the cathode was extended to the cell edge to prevent cracking from uneven heat**

	dissipation. **GTI observed little difference between cells that were impregnated sequentially with Ce nitrate and then with Cu nitrate and cells that were impregnated simultaneously. Simultaneous impregnation allowed faster cell production. Target amounts were 10 wt% CeO_2 and 20 wt% Cu in the reduced, sintered anode. Five iterations of impregnation/calcining with Ce nitrate/Cu nitrate produced 100 wt% of the target amounts. Increasing the porosity decreased the iterations necessary to reach target fill levels.** **To provide stronger and more durable cells, along with a thicker, more intact electrolyte, the anode-electrolyte tape thickness was doubled to reach the values given in Table V.** **Hg intrusion porosimetry of 250-μm thick samples representing the electrolyte was conducted and casting formulation modified to ensure electrolyte densification to a level <5%.**

Figures 1 and 2 show SEM micrographs of an impregnated cell. The electrolyte was not uniform in thickness, but did not appear to have any through pores (pinholes) or other discontinuities.

EDX analysis indicated that Cu and Ce formed uniformly throughout the thickness of the anode.

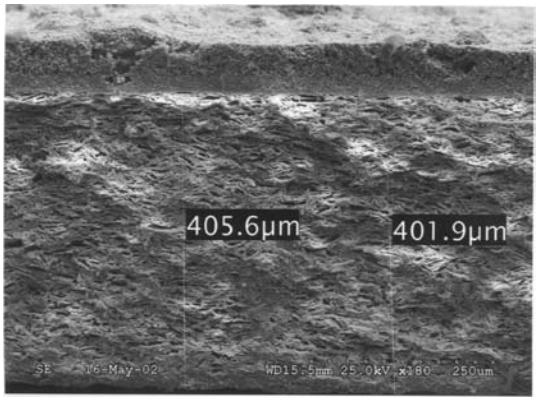

Figure 1. SEM (180X) of a Cross Section of a Fully Impregnated U-Penn Type Component Package Showing Anode Thickness

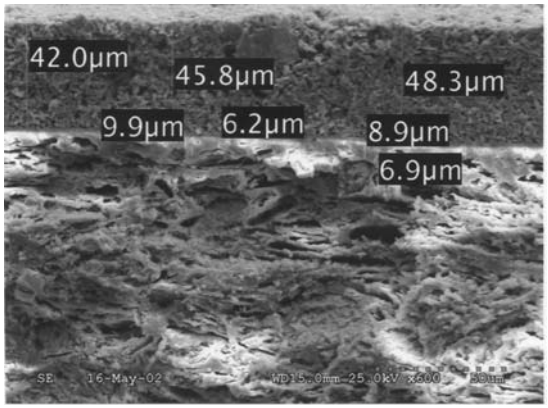

Figure 2. SEM (600X) of Fully Impregnated U-Penn Type Component Package Showing Cathode and Cathode Interlayer Thickness

Summary of Other Fabrication Procedures

Table II summarizes other fabrication procedures pursued:

Table II: Other GTI Cell Fabrication Procedures	
Method	**Comments**
2. Multiple tape cast, dense YSZ electrolyte/porous Ni-YSZ interlayer/porous YSZ tri-layer, followed by same procedures as above.	**Similar to dual tape casting. Anode interlayer and support were cast over the electrolyte. Only water-based fabrication.** **Sintered components were flat and intact; however, some migration of NiO occurred. The electrolyte was smooth and shiny with no flaws on microscopic examination. A null electronic conductivity measurement across a tri-layer - reduced out-of-cell at 700°C - indicated that NiO migration had not affected electrolyte integrity.** **Sintering multiple samples between two Al_2O_3 fiber tiles originally produced an uneven sample quality. Outer furnace samples had blue Ni aluminide circles on tiles and a bleached appearance due to Ni exiting the sample prior to the electrolyte sintering. Center samples were normal with shiny green tops and matte white bottoms. Problem was resolved by sintering only the inner furnace samples.** **After initial calcinations of Cu/Ce salts, components cracked through the center of the electrolyte and cathode, and the Cu/Ce solution leaked into the cathode. Problem was due to strain from cathode sintering when the cathode is smaller than the anode/electrolyte. Increasing the cathode area and lowering the sintering temperature from 1250 to 1230°C resolved the problem. This probably increased the cathode porosity slightly.**
3. Same as method 1 except that cathode was impregnated with Ce and Gd nitrate salts	**Cathode impregnation loadings are given in Table III below.** **The tri-layer anodes were impregnated with Cu and Ce salts after cathode impregnation.**
4. Same as method 1 except that Ag replaced Cu.	**The solution was initially too concentrated. After only one impregnation/ sintering iteration, Ag deposited on both sides of the cell. A more dilute solution of Ag and Ce nitrate could be used.**
5. Uni-axially press a mixed nano-powder zirconia with Cu_xO and ceria plus graphite pore former in a steel die to produce a 1" diameter anode.	**Bisquing to 1000°C led to a black, relatively flat and strong compact. Analysis suggested that a Cu_xO cermet formed.** **The copper color appeared to be uniform in the reduced sample.** **Attempts to spray coat this compact with nano-powder zirconia were not successful.** **Varied sintering temperature of the impregnated, sprayed bi-layer from 1150C to 1250 C and the sintering time from 4-8 hours to improve bi-layer quality. Compacts were either partially non-conductive due to Cu depletion or mechanically weak due to incomplete sintering.**
6. Tape-cast and bisque Cu_xO/CeO_2/YSZ anode followed by spray coating of the electrolyte.	**Used standard YSZ particle size for the anode.** **Sprayed layer was uneven and discontinuous, although further work might improve the quality. Spraying with nano-particle YSZ produced less Cu_xO leakage than spraying with µm-size YSZ.**

Table III gives the final cathode loadings for the cells involving cathode impregnation.

Table III: Final Cathode Loadings		
Component Number	**Number of Repetitions**	**Ce/Gd Oxide Load in Cathode**
SA042403-11	3	2.246 mg/cm^2
SA042403-12	3	2.421
SA042403-13	3	3.123
SA042403-14	11	5.333
SA042403-15	8	5.018

2.85-cm^2 Active Area, Circular, Tape-Cast, Cell Types

Table IV describes the types of cells fabricated.

Table IV: Small, 2.85 cm^2, Circular, Tape-Cast Cell Types				
Cells	**Anode**	**Electrolyte**	**Cathode**	**Comments**
"Standard" thin-electrolyte/thick anode cell.	**~600µm thick** **Geometric porosity = ~55%** **Median pore size = ~1.4 µm** **Powder size = 0.5 µm**	**~13µm**	**~100µm** **LSM/YSZ inter-layer and LSM cathode**	**Sintered bi-layers were flat before cathode application.** **Problem with cathode application.** **Impregnated cathodes sintered at 1150°C for 2 hours.**
"Standard" cell, 20-µm NiO/YSZ anode inter-layer.	**Same as above**			
"Standard" cell, cathode impregnated with 20/80-mol% Gd/Ce nitrate solution.	**Same as above**			
Thin electrolyte/thin anode	**~200µm**	**~13µm**	**~100µm** **LSM/YSZ interlayer** **LSM cathode**	**Initial fabrication activity, but cells were not tested.**
Thick electrolyte/thin anode	**~200µm** **Porosity, pore size, and powder size same as for standard cell.**	**, ~83µm**	**~46µ LSM/YSZ interlayer**	**Sintering vs. temperature and sintering vs. load tests were conducted.** **LSM layer over the cathode inter-layer omitted to preserve cell integrity.**

Bench-Scale, 3" x 4", Rectangular, Tape-Cast Cell Types

Table V: Bench-Scale, 3"x4", Rectangular Tape-Cast Cell Types			
Cells	**Anode**	**Electrolyte**	**Cathode**
"Standard" thin-electrolyte/ thick anode cell	**~600µm thick** **Geometric porosity = ~55%** **Median pore size = ~1.4 µm** **Powder size = 0.5 µm**	**~13µm**	**~100µm** **LSM/YSZ inter-layer and LSM cathode**
Comments: **Electrolyte: Cast 2-mil (50-µm)-thick, degassed, water-based, Tosoh, 8YSZ slurry onto glass.** **Anode: Cast 60-mil (1500-µm) thick, degassed, water-based slurry, containing Tosoh, 8YSZ and 30-wt % pore former (1 µm graphite flake) over the electrolyte. Removed the dried bi-layer from the casting substrate and cut. Placed cut piece between ceramic fiber tiles and sintered, reducing final length by width dimensions from 130 mm by 80 mm to 105 mm by 65 mm. Some pieces broke because 300g sintering load prevented gases from venting. Sintering without load fixed problem.** **Cathode: Painted one layer of cathode interlayer slurry (50 weight % LSM + 50 % YSZ-8 in ethylene glycol) over a 65 mm by 55 mm portion of the electrolyte. Dried at 160°C for 15 minutes. Repeated painting and drying twice more using the cathode slurry. Sintered painted sample on a ceramic fiber tile.** **During sintering, the bilayer cracked in several places along the short axis - due to stresses built up from dissimilar heat transfer for the black cathode and white electrolyte. Problem was resolved by extending the cathode to the outside edges of the electrolyte so that the top surface had no white areas exposed.** **Impregnated anode with concentrated, aqueous Cu and Ce nitrate. Evaporated the water at 110°C, causing the Cu- and Ce nitrates to crystallize in the pores of the anode. Repeated this step once. Then decomposed the nitrates to their respective oxides by heating. Repeated impregnation until the anode contained enough Cu- and Ce oxide to obtain 70 wt-% 8YSZ, 20 wt-% Cu, and 10 wt-% CeO_2. Cooled pieces to ambient prior to application of nitrate solution to prevent thermal shock.**		

2.85-cm^2 Active Area, Die-Pressed, Cell Types

Table VI: Die-Pressed Cell Types	
Uniaxially Pressed Anodes	**Comments**
Anode, containing nano-powder YSZ, Cu oxide, ceria and graphite pore former	**Complete cells were not fabricated.** **Northwestern U. (S. Barnett) evaluated 2 samples as substrates for sputtering of inter-layer and electrolyte below melting point of Cu oxide. NWU samples sintered at 1200C for 8 hrs** **NWU indicated that further work was needed to reduce surface roughness and improve inter-particle bonding.**

Tests Based on GTI – University of Pennsylvania Interaction

Table VII describes tests to minimize carbon formation and improve the reproducibility of the results, based on discussions with U-Penn.

Table VII: Tests Based on Interactions with U-Penn	
Tests	**Comments**
Application of Au ink and screen to anode and Pt ink and screen to cathode.	**Attempted to reduce contact resistance. Used on standard cells.** **Pt was sintered at 950°C and Au was sintered at 850°C to set the inks.** **This procedure significant improved OCV (see cells 03-26 and 03-30 in the results and discussion section.**
Fabrication and testing procedures at U-Penn, (9/15-19/2003).	**Obtained V-I curves and AC impedance plots for a U-Penn cell.** **Obtained SEM micrographs for a typical U-Penn cell showing the bimodal porosity with very large pores (~90 μm) in the anode.** **Obtained OCV and performance data for a good U-Penn cell.**
Hg intrusion porosimetry comparison of U-Penn and GTI anodes.	**GTI anode: single-mode pore distribution; 55.1% porosity; and 1.4-μm, median pore size.** **U-Penn anode: bi-modal pore distribution; 73.5% porosity; and 8.3-μm, median pore size.**
U-Penn cell and hardware in a GTI test stand adapted for U-Penn cell area.	**A 0.33-cm^2 active-area cell brought back from U-Penn was cemented to hardware following U-Penn procedures. In the cell test, a thin, Ag wire lead lost contact with an Ag wire cathode current-collecting loop after 1-3 days.** **In tests with a thicker Ag wire lead, the Ag wire lead did not break, but the thin Ag wire loop attached to the cathode with Ag ink broke in <150 hours.**
GTI cells cut to U-Penn cell dimensions and sent to U-Penn for evaluation.	**8 bi-layers prepared, 4 "standard" and 4 "thick electrolyte/ thin anode." 2 each impregnated simultaneously with CeO2 and Cu. 2 each impregnated first with ceria, then Cu. Cell widths were 20 mm un-sintered and 15mm sintered.** **A U-Penn test of a "standard cell showed no more carbon deposition than typically seen with U-Penn cells.** **U-Penn suggested that GTI use thicker electrolytes, as the performance advantage of thin electrolytes is minimal and the samples have little durability and strength.** **Cathode was 1 inter-layer and 2 LSM layers with drying between each layer.** **A ¾" diameter cathode was applied to the standard bi-layers, and a cathode not-quite-to-the-edge was applied to the thick electrolyte/thin anode.**
GTI-prepared, green, bi-layers sent to U-Penn for U-Penn to prepare cells and evaluate.	**2 bi-layers of "standard" and "thick electrolyte/ thin anode" tapes each were sent to U-Penn.**
Metallic impurities in the alumina cell hardware that might catalyze carbon formation.	**Coors AD-998 extruded alumina tubing material analysis: Al_2O_3 = 99.80%; SiO_2= 0.08%; CaO = 0.05%; MgO = 0.05%; FeO_2 = 0.02%; Na_2O = 0.02%.** **Coors Ceramic Company indicated that impurity levels were too low to catalyze carbon formation.**

GTI cells made with U-Penn style tape and YSZ support, but GTI areas, processing and testing. **Implementation of the U-Penn high porosity tape was still under investigation at the end of the project.** **Fabrication of both U-Penn and GTI area cells was planned.**	**YSZ tapes with a U-Penn formulation (2 pore formers - graphite powder and PMMA) were cast. The anode/electrolyte bi-layer was dual tape cast in the normal manner and then a YSZ support tape was added to the anode side of the bi-layer by slurry coating.** **The bi-layer dried flat, smooth, and free of flaws and cracks. However, surfaces had occasional smooth, round depressions, or divots, from electrolyte sinking into large pores in the anode. The optical microscope showed no cracks or discontinuities in the electrolyte, even around the divots.** **Bi-layers, sintered without a cover tile, warped with the outside edges turning under toward the anode. Bi-layers sintered with a cover tile and at a lower heating rate to organic burnout temperature were smooth and flat, but divots still formed. This procedure increased porosity to ~70%. Average thickness was only 370 μm.** **SEM of 2 bi-layers, one sintered at 4 and the other at 8 hours at 1550°C showed: (1) large, heavy PMMA particles had burrowed into the electrolyte, leaving a thin piece of electrolyte (~5 μm) below the pore; (2) PMMA had pushed out the bottom edge of the electrolyte, so it was no longer flat. The pore-former probably affected the whole area of the electrolyte. Possible solutions were to fabricate thicker (3-4x) anode and electrolyte layers or find a smaller, lighter grade of PMMA.** **Standard size (3/4") and "not-quite-to-the-edge" (~1") cathodes were painted onto the sintered bi-layers. Two layers of 50% LSM/ 50% YSZ were applied. The cells were sintered to 1230°C to protect from damage by the cathode.** **The final cells warped, but did not break after cathode application for both procedures. SEM/EDX of the cathode showed that the LSM had penetrated through the electrolyte, leaving a light brown stain through to the anode.** **Analysis of the PMMA and graphite pore formers and cathode interlayer powder (50 wt% LSM, 50 wt% YSZ) did not reveal any contaminants.**

Test Procedures

The cathode side of the electrolyte was cemented to a large alumina tube using high temperature cement so that the cathode is neatly enclosed within the tube. The layer of cement was thin to prevent extrusion onto the cathode and interfere with cathode/screen contact.

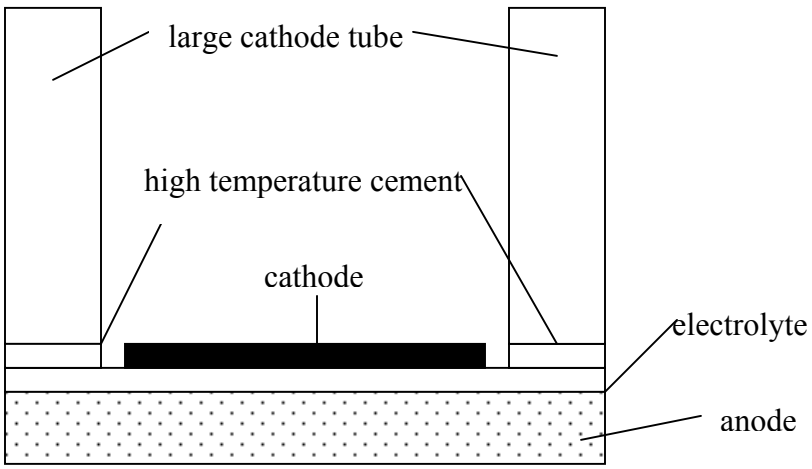

After drying over night, the anode tube/collar hardware was fitted into the test stand. The cell/cathode tube assembly was placed into the anode hardware with a talc-mica-talc gasket set between the anode tube and the anode, making sure all of the tubes are aligned in parallel for good gas sealing. The rest of the ceramic hardware and metallic screens/current collectors were added. The cell/hardware was enclosed with a small clamshell furnace.

Starting gas flows were H_2 at 100 cc/min and air at 100 cc/min. Both gases flowed through water-bubbler humidifiers. During heat-up, the humidifiers were at room temperature, providing 3% water to the gases.

The cells were heated to 700°C in 24 hours (0.5°C/minute). If desired, the same heating rate continued to 800°C. Current/voltage polarization runs were typically obtained daily once the cell reached operating conditions.

Test Stand

Figure 3 describes the test stand used for the 2.85 cm^2-area cell tests. No edge seals were used during the tests. Various gasket seals were used. These will be listed in the Results and Discussion section.

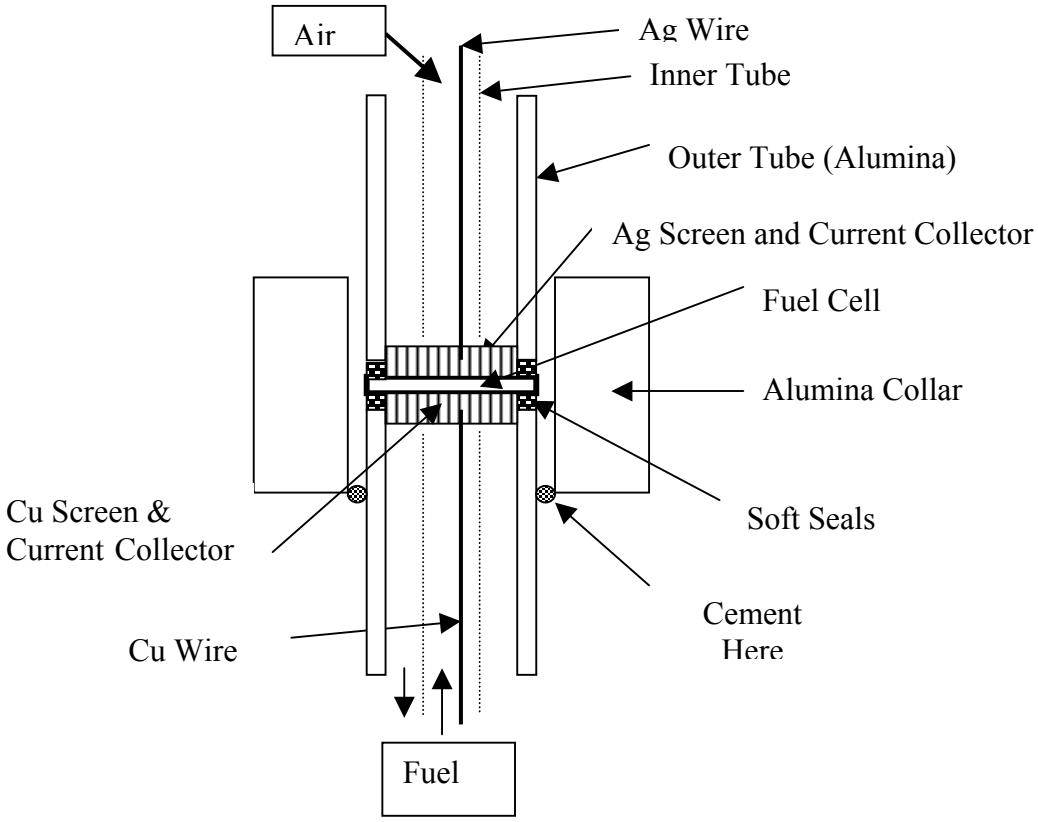

Figure 3: Cell Test Stand

RESULTS AND DISCUSSION

Thin-Electrolyte ("Standard") Cells at 800°C

Table VIII lists the tests performed on standard, thin-electrolyte cells at 800°C in terms of objectives, fuels, cell components, and test station. The tests are referenced by a test # and a component # that indicate the tape used in cell preparation.

The test stations listed correspond to three levels of humidification. All tests with H_2 included 3% water vapor to stabilize the OCV. Tests conducted in stand 4 included the ability to use completely dry hydrocarbon fuels.

Various seal materials were investigated. As of the end of the project, a fully satisfactory seal was not identified. Cement seals performed well but did not survive thermal cycling. The talc-mica-talc seals could be thermally cycled but no cell using these seals reached theoretical OCV, indicating some leakage. Edge seals were not employed.

Fuels included dry H_2, humidified H_2, dry CH_4, humidified CH_4, N_2-diluted CH_4, CH_4 with sulfur compounds, N_2 and CH_4 with sulfur compounds, and as-received dry natural gas.

All of the tests used 1" diameter anode/electrolyte bilayers on to which a 0.75" diameter cathode was painted. Therefore, the anode had an area of 5 cm^2 of which only ~2.85 cm^2 was directly exposed to fuel. All 2.85 cm^2 of the cathode was exposed to oxidant. One bench-scale cell was tested which had a 3" x 4" active area.

Tests were conducted for reasons relating to varying the test stand configuration, evaluating different fuels, using different cell materials and fabrication procedures, operating under different conditions, and measuring cell performance differently.

Table IX provides the operating lifetime and degradation effects in the cell tests. The table indicates: (1) the cell sometimes broke during testing; (2) extensive carbon often formed; (3) less frequently, copper segregation occurred, (4) conditions (e.g., power outage, thermal cycle) often changed during testing. These effects complicated, but did not prevent, interpretation of cell performance data.

Table X provides the electrochemical performance of the cells in terms of the maximum power density produced from steady state operation, the maximum power density produced during polarization runs, the change in OCV with time, and the change in steady-state performance over time. In the "Performance Change Over Time" column, the numbers refer to voltage (in mV) change under constant load except when "current" is included. In the "current" cases, the readings refer to current (in mA) at a constant 0.5V. In most cases, the polarization data are comparable to or somewhat higher than the operating data because the operating data is not always occurring at the maximum power point.

Electrochemical Performance

The variability in the results is indicative of the complicating factors cited above. The overall power densities on H_2 fuel did not exceed 115mW/cm^2. The power densities obtained with dry CH_4 and natural gas were generally ~50% or more lower than those obtained with H_2. However, a few cells (03-03, 03-08, 03-22, 03-27) produced power densities on CH_4 that were similar to, or higher than, those obtained with H_2. Addition of the Ni/YSZ interlayer resulted in cells (03-13, 03-20, and 03-21) with power densities up to 93 mW/cm^2 on H_2 and 36 mW/cm^2 on dry CH_4.

Table VIII: Objectives and Components for "Standard" Cell Tests at 800°C

[Unless otherwise noted: ~600 μm anode impregnated with 20%Cu/10%ceria, ~13 μm electrolyte, ~100 μm m LSM, Cu screen/contact lead on anode and Ag screen/contact lead on cathode. Oxidant is air with 3% H2O.]

Test #	Objective	Fuel	Component # and Impregnation	Test Station	Anode Seal	Cathode Seal
02-20	Compare performance of cells with simultaneously and sequentially impregnated Cu and CeO_2.	H_2/3% H_2O	SA052002-13 Sequential	s-3	talc-mica-talc	cement
02-24	Compare C deposition on load with N_2-diluted, dry CH_4, containing 75-ppm S compounds to C deposition with previous Cu cells.	H_2/3% H_2O	SA052002-12 Sequential	s-4	talc-mica-talc	cement
		50% N_2/50% CH_4 (75 ppm sulfur compounds)				
02-25	CH_4 diluted with N_2	H_2/3% H_2O	SA052002-13 Sequential	s-4	talc-mica-talc	cement
02-26	CH_4 diluted with N_2	H_2/3% H_2O	SA052002-14	s-4	talc-mica-talc	cement
		50%N2/50%CH4				
03-01	"Upside Down" test-cemented anode to mimic UPenn configuration.	H_2/3% H_2O	SA050202-17	s-4	cement	none
		Dry CH_4				
03-03	Constant voltage (compared to constant current) test, N_2 around outside edge.	H_2/3% H_2O	SA052002-15	s-4	talc-mica-talc	cement
		Dry CH_4				
03-04	Max CH_4 flow (190cc/min) + OCV variation with time at different T's (750, 800, 700C)	Dry CH_4	SA052002-18	s-4	mica	cement
03-08	Dry CH_4 performance at constant, 0.5V with PEL, double furnace	H_2/3% H_2O	SA052002-20	s-4	talc-mica-talc	cement
		Dry CH_4				
03-09	Dry CH_4/S performance at constant, 0.5V. PEL and double furnace	H_2/3% H_2O	SA052002-27	s-4	talc-mica-talc	cement
		Dry CH_4, 26ppm COS and 47ppm tetrahydrothiophene				
03-13	~13 μm NiO/YSZ interlayer reduced under pure H_2.	H_2/3% H_2O	SA030303-2	s-3	talc-mica-talc	cement
03-20	Constant V, sulfur tolerance test, ~13μm NiO/YSZ interlayer	H_2/3% H_2O	SA052002-31	s-4	talc-mica-talc	Ultra Temp 516
		Dry CH_4				
		Dry CH_4 w 100 ppm H_2S				
03-21	Natural gas test, ~13 μm NiO/YSZ interlayer	H_2/3% H_2O	SA052002-32	s-3	talc-mica-talc	Ultra Temp 516
		Dry full-spectrum Nat Gas				
03-22	Standard cell with Pyrex gaskets on constant voltage, sulfur tolerance test	H_2 w/3% H_2O	SA042403-1	s-4	Pyrex-40 mils	Pyrex-40 mils
		Dry CH4				
		Dry CH4/100 ppm H2S				
03-23	Pt ink/Ag screen on cathode side, Au ink/Ag screen on anode	H_2/3% H_2O	SA042403-2	s-3	talc-mica-talc	Ultra Temp 516
		Dry CH_4				
03-24	Pt ink on cathode side, Au ink on anode, without noble metal screens.	H_2/3% H_2O	SA042403-3	s-1	talc-mica-talc	Ultra Temp 516
		CH_4, w 3% H_2O				
03-26	Pt ink/screen on cathode, Au ink on anode	H_2/3% H_2O	SA042403-4	s-4	Ultra Temp 516	Open to air
		Dry CH_4				
03-27	Heated under short, compare to 03-29	H_2/3% H_2O	SA052002-34 sequential	s-3	talc-mica-talc	Ultra Temp 516
		Dry CH_4				
DHOX-1	3"x 4" Cu-based SOFC tri-layer package. Ni screen on anode side. 35 cm2 active area.	H_2/3% H_2O		NA	mica/glass tape	mica/glass tape

Table IX: Duration and Degradation for "Standard" Cell Tests at 800°C

Test #	Fuel	Operation (Hours)	Carbon	Cu Segregation	Comments
02-20	H_2/3% H_2O	1104	n/a	Anode is gray in active area, lighter in center, coppery under gasket	OCV/performance declined due to cracked cell package.
02-24	H_2/3% H_2O	48	Minimal	moderate	
	50% N_2/50% CH_4 (75 ppm sulfur compounds)	90			
02-25	H_2/3% H_2O	96	n/a	severe	OCV and performance decreased due to cell breaking into 6 pieces.
02-26	H_2/3% H_2O	1	minimal	moderate	Light C in anode, heavy in talc gasket. Dilution appears to decrease C.
	50%N_2/50%CH_4	113			
03-01	H_2/3% H_2O	22	extremely heavy	none visible	Cell declined rapidly on CH_4, but not on H_2. Massive C with CH_4.
	Dry CH_4	24			
03-03	H_2/3% H_2O	90	extremely heavy	severe	H_2 performance declined before switch to CH_4. CH_4 performance: 500 mV, 434 mA.
	Dry CH_4	32			
03-04	Dry CH_4	20	moderate; heavier around seal	none visible	Post test resistance measurement of 978 Ω indicated that a short due to carbon formation might have developed.
03-08	H_2/3% H_2O	22	heaviest ever (> 1/2")	none visible	
	Dry CH_4	59			
03-09	H_2/3% H_2O	72	minimal	none visible	Cell was not on OCV prior to load.
	Dry CH_4, 26ppm COS and 47ppm tetrahydro-thiophene	264			
03-13	H_2/3% H_2O	1008	n/a	none visible, anode pinkish yellow SEM/EDX of the interlayer interface showed no diffusion of Ni to the anode, even at 1500x. Inter-layer contained Cu, but no ceria.	First inter-layer cell. Pure H_2 used for reduction. Cell did not performed well after increase to 800C and outage. Because of OCV decline, cell was not run on CH_4. XRD showed that the anode contained Cu, CeO_2, and $CuYO_2$ – suggesting that poor seal might have oxidized the anode.
03-20	H_2/3% H_2O	116	minimal	none visible	Original H_2 OCV regained when switch back to H_2
	Dry CH_4	23			
	Dry CH_4, 100 ppm H_2S	284			
03-21	H_2/3% H_2O	136	moderate; heavier around seal	none visible	Terminated cell because of rapid decline in OCV and V/I. XRD showed that the anode contained Cu, CeO_2, $CuYO_2$, Cu_xO (air leakage?) and tentatively CuS_2. Cu may have reacted with odorant to a minor extent.
	Dry full-spectrum Nat Gas	37			
03-22	H_2 w/3% H_2O	296	moderate	none visible	Crashed after initial cycles on CH_4/H_2S and CH_4 on restoring to H_2. Constant V and I results. One high reading after brief outage.
	Dry CH_4	42			
	Dry CH4/100 ppm H_2S	23			
03-23	H_2/3% H_2O	452	moderate	none visible	OCV on H2 was high and const, but declines with CH4. Ink sintered and blocked pores.
	Dry CH_4	44			
03-24	H_2/3% H_2O	522	minimal; heavier around seal	none visible	H_2 OCV and V/I regained when switch back to H_2. Survived power outage and relay thermal cycle. Constant OCV on dry CH4 over short period. Ag screen melted and Au ink failed.
	CH_4, w 3% H_2O	66			
03-26	H_2/3% H_2O	306	moderate	moderate; flaky Cu layer bonded to Au screen	Performance and OCV on H_2 was not regained.
	Dry CH_4	44			
03-27	H_2/3% H_2O	92	heavy; cell broken	none visible	Cell crashed on restoring to H_2. Both constant V and constant load results.
	Dry CH_4	64			
DHOX-1	H_2/3% H_2O	168	84-76% apparent anode sealing efficiency. High contact resistance. Initial anode/cathode sealing efficiency of 84% and 95%, respectively, with a N_2 cross over of 6%. OCV and seal efficiency decreased with time due to increase in N_2 (6-9%) and H_2 cross over. GC on the fuel and oxidant outlet and condensate under OCV indicate ~21% fuel crossover into cathode. Compensating for fuel cross over, anode sealing efficiency was 94%.			

Table X: Performance for "Standard" Cell Tests at 800°C										
Test #	Fuel	Max Operating Voltage	Max Operating Current	Max Operating Power Density	Max Polarization Voltage	Max Polarization Current	Max Polarization Power Density	OCV Change Over Time	Performance Change Over Time	IR
02-20	H_2/3% H_2O	0.544	0.2	38.2	0.513	0.205	36.9	1028 to 1035	544 to 499	no
02-24	H_2/3% H_2O	0.949	0.05	16.6	0.508	0.24	42.8	n/a	n/a	no
	50% N_2/50% CH_4 (75 ppm S compounds)	0.766	0.05	13.4	0.515	0.08	14.5	895 to 817	766 to 563	no
02-25	H_2/3% H_2O	0.775	0.05	13.6	0.506	0.165	29.3	1023 to 1015	775 to 478	no
02-26	H_2/3% H_2O	1.006	0.025	8.8	0.521	0.275	50.3	n/a	936 to 1006	no
	50%N_2/50%CH_4	0.67	0.1	23.5	0.501	0.155	27.2	998 to 729	670 to 543	no
03-01	H_2/3% H_2O	0.702	0.3	73.9	0.504	0.435	76.9	1065 to 1071	650 to 702	no
	Dry CH_4	0.747	0.1	26.2	0.5	0.235	41.2	960 to 524	721 to 455	no
03-03	H_2/3% H_2O	0.588	0.4	82.5	0.499	0.47	82.3	1036 to 1015	588 to 465	no
	Dry CH_4	0.5	0.434	76.1	n/a	n/a	n/a	n/a	434 to 70 current	no
03-04	Dry CH_4	n/a	n/a	n/a	n/a	n/a	n/a	792 to 728	n/a	no
03-08	H_2/3% H_2O	0.5	0.641	112.5	n/a	n/a	n/a	n/a	641 to 621 current	no
	Dry CH_4	0.5	0.64	112.3	n/a	n/a	n/a	n/a	640 to 78 current	no
03-09	H_2/3% H_2O	0.525	0.25	46.1	0.502	0.26	45.8	1001 to 1004	507 to 525	no
	Dry CH_4, 26ppm COS and 47ppm tetrahydrothiophene	0.498	0.115	20.1	n/a	n/a	n/a	n/a	115 to 61 current	no
03-13	H_2/3% H_2O	0.579	0.425	86.3	0.504	0.475	84.0	1040 to 1023	557 to 579 to 517	no
03-20	H_2/3% H_2O	0.541	0.35	66.4	0.502	0.36	63.4	1065 to 1050 after hydrocarbons	541 to 524	230 mV @ 200 mA
	Dry CH_4	0.498	0.208	36.3	n/a	n/a	n/a	n/a	208 to 166 current	no
	Dry CH_4 w 100 ppm H_2S	0.498	0.180	31.5	n/a	n/a	n/a	1033 to 1018 to 1025	166 to 180 to 161 current	no
03-21	H_2/3% H_2O	0.499	0.532	93.1	0.5	0.525	92.1	1043 to 1035 (change const I to const V)	532 to 452 current	160 mV @ 300 mA
	Dry Natural Gas	0.499	0.286	50.1	n/a	n/a	n/a	907 to 587	286 to 20 current	
03-22	H_2 w/3% H_2O	0.551	0.2	38.7	0.5	0.22	38.6	1023 unchanging	552 to 548	no
	CH_4 w/3% H_2O	0.499	0.198	34.7	n/a	n/a	n/a	934 to 956	106 to 198 current	no
	Dry CH_4/100 ppm H_2S	0.499	0.08	14.0	0.5	0.073	12.8	989 unchanging	76 to 72 to 80 current	no
03-23	H_2/3% H_2O	0.498	0.513	89.6	0.498	0.48	83.9	1049 to 1050 (931 after CH_4)	513 to 257 current	no
	Dry CH_4	0.498	0.237	41.4	0.51	0.195	34.9	957 to 809	237 to 204, 164 to 204 to 188	no
03-24	H_2/3% H_2O	0.593	0.275	57.2	0.5	0.337	59.1	1030 to 1031	593 to 544	no
	CH_4, w 3% H_2O	0.705	0.1	24.7	0.511	0.175	31.4	no	594 to 634	no
03-26	H_2/3% H_2O	0.548	0.25	48.1	0.498	0.285	49.8	1089 to 1079	569 to 546	no
	Dry CH_4	0.567	0.05	9.9	0.498	0.055	9.6	890 single point	567 to 473	no
03-27	H_2/3% H_2O	0.586	0.125	25.7	0.502	0.15	26.4	998 to 960 896 after CH_4	586 to 580	no
	Dry CH_4	0.723	0.125	31.7	0.5	0.235	41.2	1002 to 950	539 to 723	no
DHOX-1	H_2/3% H_2O	n/a	n/a	n/a	0.543	0.114	62			

Many factors affecting the power densities obtained are discussed later in this report. Further work to resolve these issues should significantly improve the power densities. The power densities tended to be somewhat lower than those cited in the literature for H_2 and hydrocarbons such as propane or butane. Relatively little data is available for dry CH_4 and natural gas with Cu/ceria/YSZ anodes (see however, Park, S. et al, 2004; Lu, C. et al, 2002; Kim, H. et al, 2002; McIntosh, S. et al, 2003).

Table X indicates that the OCV most commonly was stable when a cell operated on H_2, but declined – sometimes rapidly – after switching to hydrocarbon fuel. However, a few standard cells (03-20, 03-22, 03-27) had relatively stable OCVs on CH_4. OCV stability also increased when methane was humidified. Tables IX and X, taken together, suggest that the OCV decline may correlate with carbon formation. Carbon deposits may have compromised the integrity of the cell by causing cracking, increased leaking, electrical shorting, or blocking fuel oxidation, leading to OCV changes.

A post-test resistance measurement across the cell for cell 03-04 as well as an earlier cell, produced low resistances in the range of 500 – 978 Ω, while a cell operated only on H_2 had a resistance if ~800,000 Ω. This is consistent with electrical shorts developed across the cell due to carbon deposits. The OCV would be expected to decline as these shorts grew over time.

Flow tests and analysis conducted after the project ended also supported the possibility that pinholes or shorts were contributing to the OCV decline. The OCV declined as the fuel and oxidant flow rate declined because a short was consuming more fuel or fuel dilution from leaking pinholes increased.

The electrical performance of the cells declined as the OCV declined on CH_4. Whereas cells operating on H_2 were operated for >1000 hours, cells operating on CH_4 only operated up to ~70 hours and resulted in poor "end of life" electrochemical performance.

Carbon Formation and the Effect of Sulfur Compound Addition

Some carbon deposition was observed on all tests conducted with methane fuels. In some tests, extensive carbon deposits physically disrupted the cell. Carbon can form either by CH_4 cracking or CO disproportionation (the Boudouard Reaction).

$$CH_4 \rightarrow C + 2\ H_2$$

$$2\ CO \rightarrow C + CO_2$$

CO can form by the reformation or partial oxidation of CH_4 either on the anode or by a gas phase reaction between water vapor or air infiltrating through the perimeter seals or the electrolyte.

Many factors may have contributed - alone or in combination - to form carbon. Investigation of these factors was continuing at the end of the project. They include:

- Poor seal integrity and resulting ingress of O_2 or water vapor into the anode. The experimental section showed that the GTI test stand is a tube-against-tube arrangement, with the tubes separated by the gasket seals and cell. This arrangement differs from small cell test arrangements often cited in the literature for testing dry hydrocarbons. These arrangements typically seal the cell to a single tube on the anode side and omit a tube for controlling airflow on the cathode side. Alignment and contact issues with the tube-against-tube arrangement may have contributed to seal leakage and increased the tendency for carbon deposition. In support of this, a significant number of cells were

unable to reach theoretical OCV on H_2/air. Also, more carbon deposition was observed in the seal areas as well as in the anode.

- Poor electrolyte integrity causing cross over from the cathode. This could have been a consequence of the very thin electrolytes used to increase power density. Pinholes through the electrolyte could serve as a location for carbon deposition and shorting.
- Gas-phase C deposition. This is known in the literature, and might have been enhanced in our tests due to seal and/or electrolyte leaks.
- Trace contaminants in the cell or test fixture. It was suggested that the alumina tubing used to supply gas to the anode may itself catalyze carbon deposition. There was some evidence of carbon deposition on the alumina upstream and downstream of the cell.
- Temperature. Carbon deposition might have been increased if the temperatures in GTI cells were higher than those in the literature. No evidence for this option is available.

Tests on standard cells 03-08 and 03-09 compared carbon formation using dry CH_4 and dry CH_4 containing sulfur compounds, respectively.

The cells were heated to 700°C and operated for a few days on H_2/3% water vapor. The OCV was monitored to estimate seal and electrolyte integrity. A cell with perfect seals and a pinhole-free electrolyte should have an OCV of 1100 mV under these conditions. Since the anode is porous all the way to its outer edges, the seal is not perfect. The cells were then switched to dry CH_4 or dry CH_4 with sulfur compounds added, respectively.

Figure 4 shows the comparative performance of both of these cells on methane fuel.

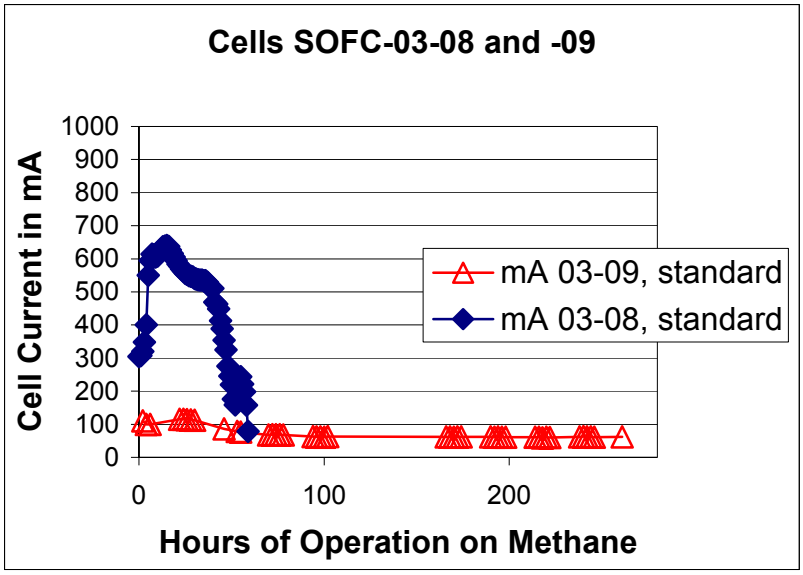

Figure 4. Performance Plots for Cell -03-08 Operating on Pure Dry Methane and Cell -03-09 Operating on Methane with 75 ppm Sulfur Compounds at 800°C

Cell SOFC-03-08 had an OCV of 1047 mV and a maximum power density of 45.6 W/cm^2 on H_2/air and at 700°C and a power density was 112.5 W/cm^2 at 800C – the second highest value obtained. The power density lost about half its value on switching to CH_4, but then regained all of the lost power density after 15 hours. The cell then decayed rapidly. Upon disassembly,

heavy carbon had formed at the anode/current collector interface sufficient to warp the copper current collector and disrupt and crack the cell.

The literature has indicated that behavior similar to that of cell 03-08 is indicative of carbon formation causing an initial improvement in anode conductivity followed by pore blocking that limits gas transport (McIntosh, et. al.).

Cell SOFC-03-09 exhibited an open circuit voltage of 1048 mV on H_2/air at 700°C, but a much lower power density of ~46 mW/cm^2 at 800C. Current interrupt measurement indicated that the cell had a high internal resistance of 3.2 Ω. Increasing the holding force on the cathode current collector decreased resistance and increased performance slightly. The test was continued despite the high contact resistance. Post-test analysis showed that the cathode current collector was deformed slightly and was not making good contact.

Operation on dry CH_4 containing 25 ppm carbonyl sulfide and 50 ppm tetrahydrothiophene with a cell voltage was maintained at 500 mV using a constant load device, reduced the power density to 20 mW/cm^2 initially and then to 11 mW/cm^2. However, then the cell operated stably for the final seven days. Upon disassembling the cell, no large carbon deposit was observed although minor amounts of carbon had deposited on the ceramic hardware and on the anode hardware.

Figure 5 is a photo showing the some of the post-test hardware from both cells.

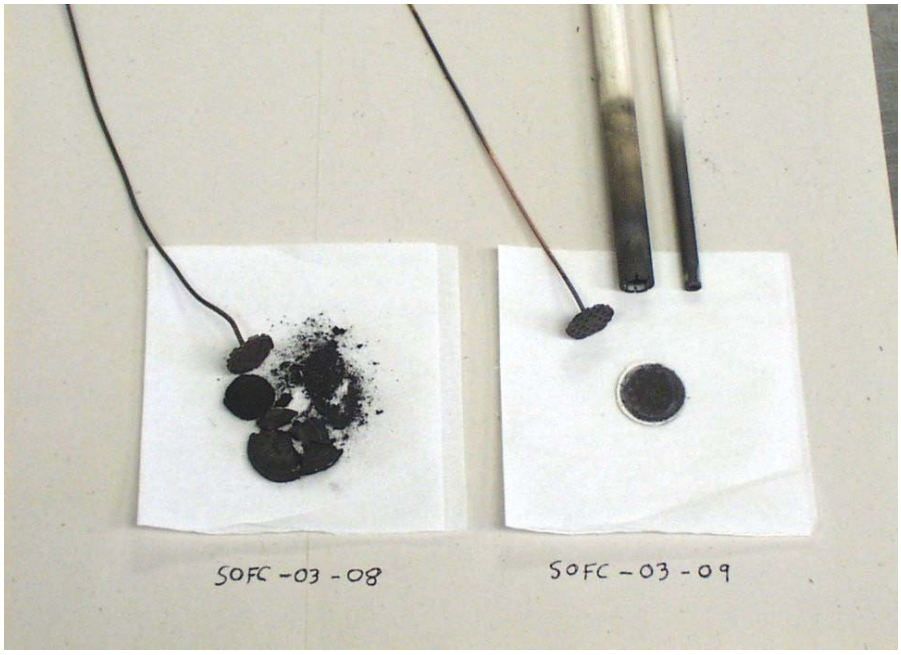

Figure 5. Photograph showing hardware from Cells 03-08 and 03-09, including the anode current collector and bulk of the carbon deposit from Cell 03-08 and the anode current collector, the cell (anode side up), and two of the three concentric alumina tubes used to supply methane to Cell 03-09.

The small inner ceramic tube (right side) from Cell 03-09 was located inside the larger ceramic tube and used to hold the copper current collector against the anode. CH_4 was admitted through the interior of the larger tube and exited around the outside. The carbon deposited on the small inner tube adhered strongly to the tube and also was electrically conductive. Alligator clips positioned 1-cm apart on the blackened portion of the small ceramic tube indicated an electrical resistance of about 800 Ω. Both the adherence and the electrical conductivity indicated that the

deposit was graphitic and not due to a gas phase reaction. Its position on the inner tube, upstream of the cell, is consistent with methane cracking since no carbon monoxide should be present in the gas flow at this point. The outside of the larger tube contains a similar deposit that is also strongly adherent and electrically conductive.

Cell 03-08, on the other hand, was completely disrupted by free-carbon deposits. The physical nature of this carbon was consistent with soot formation suggesting the Boudouard reaction as a source. The carbon appeared to have formed at the anode/current collector interface pushing the current collector away from the cell with enough force to crack the cell around the perimeter seals, allowing crossover of air and fuel through the cracks.

Approximately four grams of carbon were recovered from Cell 03-08. The total current flowing through Cell 03-08, while on methane, was 28.8 amp-hours or about 104,000 Coulombs – enough to form about one gram of carbon via the combination of the electrochemical oxidation of methane and the Boudouard Reaction.

$$2\,CH_4 + 6\,O^{2-} \rightarrow 4\,H_2O + 2\,CO + 12\,e^-$$

$$2\,CO \rightarrow C + CO_2$$

The additional three grams of carbon could have formed from methane partial oxidation via direct reaction of the fuel and oxidant after the cell integrity was compromised.

Cell SOFC-03-09 began life with a higher internal resistance due to poor contact between the cathode and its current collector. A small initial increase in performance may be due to carbon depositing. However, the contact resistance and the little amount of carbon formed may have limited performance improvement.

Little carbon may have formed in cell 03-09 because of the carbon inhibition by carbonyl sulfide and tetrahydrothiophene or possibly a current density effect. Sulfur inhibition may be the most likely effect. It is well known that the presence of sulfur inhibits the Boudouard Reaction in steam reforming of hydrocarbons thus permitting a lower steam to hydrocarbon ratio. Additional work is required to understand what conditions favor carbon deposition and what conditions inhibit it.

Significant life extension appears possible at 800C for cells operating on dry methane contaminated with 75 ppm sulfur. Cell 03-020 also operated stably at 800C for two cycles of ~200 hours on dry methane and 100 ppm H_2S followed by ~100 hours on H_2. Cell deteriorated during third such cycle, possibly due to gradual affect of inadequate sealing. Carbon formation was minimal. Thus two standard cells with added sulfur operated much longer than cells operated with dry CH_4 alone at 800C (~70 hrs).

Effect of Sulfur on Power Density

Cells 02-24, 03-09, 03-20, 03-21, and 03-22 involved methane fuels that contained sulfur compounds. Typically ~75-100 ppm of sulfur compounds were added to the fuel. In cells 03-20 and 03-22, carbon deposition from initial operation on CH4 alone could have influenced the power density obtained after the addition of sulfur.

The test results varied with respect to the effect of sulfur. For example, the power densities of cell 03-20 were similar on CH_4 and CH_4 with 100 ppm of H_2S, whereas cell 03-22 lost 75% of its power when H_2S was added. Work beyond the scope of this project will be needed to determine the effect of sulfur on power density.

Bench-Scale Cell

DHOX-1 was the first test to use the larger-area cell in a GTI-designed test stand. The cell contained: 35 cm^2 planar active area, mica/glass tape seal gaskets, and nickel and silver screen current collectors.

Operation: The cell was heated in 24 hours using 200 sccm of H_2 and 793 sccm air (oxidant). These flows correspond to 53 % fuel and 32 % oxidant utilizations at 1 atm and a current density of 400 mA/cm^2. Fuel and oxidant were humidified at room temperature. The cell improved for ~l20 hours due to a decrease in contact resistance, IR (from 18-14 mohms) and polarization and thereafter was stable. Initially, the cell exhibited anode and cathode sealing efficiencies of 84% and 95%, respectively, with a N_2 cross-over of 6% and an OCV of 1052mV (49 mV lower than the theoretical value at 800°C). Both OCV, anode and cathode seal efficiencies decreased with time due to an increase in N_2 (6-9%) and H_2 crossover. From the GC analyses of the fuel and oxidant outlet streams and condensate (anode and cathode) collection rate data under OCV conditions, the fuel crossover into the cathode was estimated to be ~21%. Based on this analysis and compensating for the fuel cross-over, the adjusted anode sealing efficiency was determined to be 94% suggesting that mica/glass combination provides good sealing in SOFC testing.

The cell reached a maximum power density of 62 mW/cm^2 at 114mA/cm^2 (543 mV) and H_2 and air utilizations of 15 and 9 %, respectively. This performance resembled that obtained in 3-cm^2 cell tests under similar conditions. The low performance is attributed to the low apparent anode sealing efficiency (84-76%), high fuel and oxidant gas crossover and contact resistance. Dry methane oxidation was not investigated due to the high cross over rates.

Post-test examination: No cracking was observed after the anode flange was removed. However, the seal area was covered with mica, so any micro-cracks or hairline cracks would not have been seen. The cathode and cathode screen were extremely well bonded to each other and to the cathode flange, so that removing it destroyed the component package. XRD showed that the anode surface contained only copper and cerium oxide, despite the various colors observed.

Thin-Electrolyte ("Standard") Cells at 700°C

Tables XI - XIII summarize the tests performed on standard, thin-electrolyte cells at 700C in a manner similar to the tables VIII – X for tests on standard cells at 800C. 700C operation was expected to reduce carbon deposition at the cost of reduced power density.

Electrochemical Performance and Carbon Formation

Power densities at 700C were significantly lower than those obtained at 800C. The overall power densities on H_2 fuel did not exceed 40mW/cm^2. The power densities obtained with carbon fuels - CH_4, odorized natural gas, and simulated reformate - did not exceed 15 mW/cm^2.

Only two Ni/YSZ interlayer cells (03-13 and 03-15) were tested at 700C. One failed within a day; the other cell produced 39.5 mW/cm^2. As with the 800C results, a number of non-interlayer cells closely approached this output. The benefit of an inter-layer may only take effect in cells with more optimized microstructures.

Table XI: Objectives and Components for "Standard" Cell Tests at 700°C

[Unless otherwise noted: ~600 µm anode impregnated with 20%Cu/10%ceria, ~13µm electrolyte, ~100 µm LSM, Cu screen/contact lead on anode and Ag screen/contact lead on cathode. Oxidant is air with 3% H_2O.]

Test #	Objective	Fuel	Component # and Impregnation	Test Station	Anode Seal	Cathode Seal
03-04	Max CH_4 flow (190cc/min) + OCV variation with time at different temperatures	Dry CH_4	SA052002-18	s-4	mica	cement
03-06	Variation of OCV with time.	Dry CH_4	SA052002-19	s-3	talc-mica-talc	alumina cement
03-10	Dry CH_4 and N. G. performance at constant, 0.5V, PEL)	H_2/3% H_2O	SA052002-28	s-3	talc-mica-talc	cement
		Dry CH_4				
		Dry odorized NG (93% CH_4)				
03-13	Dry CH_4 at OCV and 0.5V ~13 µm NiO/YSZ interlayer reduced under pure H_2	H_2/3% H_2O	SA030303-2	s-3	talc-mica-talc	cement
03-14	Test the use of standard cement on both air and fuel sides of the cell	H_2/3% H_2O	SA052002-29	s-1	cement	cement
03-15	Tape-cast interlayer, cell reduced under mixed H_2/N_2 gas	H_2/3% H_2O	SA030303-4	s-1	talc-mica-talc	cement
03-16	Cell cemented on the cathode side with Zr cement/fiber (E. Ong)	H_2/3% H_2O	SA052002-30	s-1	talc-mica-talc	zirconia cement/ fiber
03-18	Ce/Gd impregnated cathode	H_2/3% H_2O	SA052002-36	s-4	talc-mica-talc	Ultra Temp 516
03-19	Ce/Gd impregnated cathode	H_2/3% H_2O	SA052002-37	s-4	talc-mica-talc	Ultra Temp 516
03-23	Pt ink/screen on cathode side, Au ink/screen on anode	H_2/3% H_2O	SA042403-2	s-3	talc-mica-talc	Ultra Temp 516
		Dry CH_4				
03-24	Pt ink on cathode side, Au ink on anode, without noble metal screens.	H_2/3% H_2O	SA042403-3	s-1	talc-mica-talc	Ultra Temp 516
03-25	Ce/Gd impregnated cathode in standard cell with 2.4 ppm/cm^2 of Ce/Gd oxide	H_2/3% H_2O	SA042403-12	s-4	talc-mica-talc	Ultra Temp 516
03-26	Pt ink/screen on cathode, Au ink on anode	H_2/3% H_2O	SA042403-4	s-4	Ultra Temp 516	Open to air
		Dry CH_4				
03-27	Separately impregnated, heated under short, compare to 03-29	H_2/3% H_2O	SA052002-34 separate	s-3	talc-mica-talc	Ultra Temp 516
03-29	Heated under OCV	H_2/3% H_2O	SA052002-35 separate	s-4	talc-mica-talc	Ultra Temp 516
		Dry CH_4				
03-30	Heated under short, Pt ink/screen on cathode side, Au ink/screen on anode	H_2 w/3% H_2O,	SA042403-5	s-3	Ceramabond 552	open to air
		Dry CH_4,				
		58%H_2/22%CO_2/20%H_2O				

Table XII: Duration and Degradation for "Standard" Cell Tests at 700°C					
Test #	**Fuel**	**Operation (Hours)**	**Carbon**	**Cu Segregation**	**Comments**
03-04	Dry CH_4	90 CH_4	moderate; heavier around seal	none visible	Post test resistance measurement of 978 Ω indicated that a short due to carbon formation may have developed.
03-06	Dry CH_4	264	Minimal	none visible	
03-10	H_2/3% H_2O	192	minimal; heavier around seal	none visible	27.5 W/cm^2 constant I on H_2.
	Dry CH_4	455			
	Dry odorized NG (93% CH_4)	48			
03-13	H_2/3% H_2O	1200	n/a	none visible, anode pinkish yellow	First inter-layer cell. Pure H_2 used for reduction. Cell did not performed well after increase to 800C and outage. Because of the OCV decline, cell was not run on CH_4. XRD showed that the anode contained Cu, CeO2, and CuYO2 – suggesting that inadequate sealing might have led to oxidation of the anode. SEM/EDX of the anode interlayer interface showed no diffusion of Ni from the interlayer to the anode, even at 1500x. Inter-layer contained Cu, but no ceria.
03-14	H_2/3% H_2O	2	n/a	minimal, copper also in cement seal	Failed in 2 hours. OCV was very unstable and dropped suddenly. Cell cracked, due to the cement seal. The cell also had poor contact.
03-15	H_2/3% H_2O	22	n/a	none visible	Failed. Severe fluctuations. A temperature controller failed. Cell sealing was poor with no cement-component bond.
03-16	H_2/3% H_2O	101	n/a	none visible	Failed because the seal cement was porous; the anode oxidized around its outer edge.
03-18	H_2/3% H_2O	5	n/a	none visible	Failed in 5 hours due to cracked cell and/or seal.
03-19	H_2/3% H_2O	5	n/a	none visible, anode yellow brown	Failed due to poor OCV and cracked seal by heating with tightened bolts.
03-23	H_2/3% H_2O	882	moderate	none visible	OCV on H_2 was high and const, but declines with CH_4. Ink sintered and blocked pores.
	Dry CH_4	66			
03-24	H_2/3% H_2O	72	n/a	none visible	Good OCV on H_2 and constant OCV on dry CH4 over short period. Repeated, thermal cycles due to a failing controller/furnace heater, caused Ag screen to melt and Au ink on the anode to fail.
03-25	H_2/3% H_2O	0	n/a	none visible	Failed due to extreme instability due to terrible seal; cement failed.
03-26	H_2/3% H_2O	962	moderate	moderate; flaky Cu layer bonded to Au screen	Performance and OCV on H_2 was not regained. At termination cell was deteriorating.
	Dry CH_4	32			
03-27	H_2/3% H_2O	24	n/a	none visible	Cell crashed on restoring to H2. Both constant V and constant load results.
03-29	H_2/3% H_2O	744	minimal; heavier around seal	significant	Terminated when cell became unstable, OCV dropping. Layer of copper "foil" bonded to Cu screen.
	Dry CH_4	312			
03-30	H_2 w/3% H_2O,	222	minimal amount only near seal	none visible	Terminated when cell became very unstable.
	Dry CH_4,	356			
	58%H_2/22%CO_2/20%H_2O	44			

Table XIII: Performance for "Standard" Cell Tests at 700°C										
Test #	Fuel	Max Operating Voltage	Max Operating Current	Max Operating Power Density	Max Polarization Voltage	Max Polarization Current	Max Polarization Power Density	OCV Change Over Time	Performance Change Over Time	IR
03-04	H_2/3% H_2O	0.72	0.1	25.3	0.503	0.165	29.1	1043 to 1055	765 to 720	no
	Dry CH_4	n/a	n/a	n/a	n/a	n/a	n/a	614 to 576	n/a	no
03-06	H_2/3% H_2O	0.659	0.15	34.7	0.501	0.21	36.9	1054 to 1053	659 to 645	no
	Dry CH_4	n/a	n/a	n/a	n/a	n/a	n/a	907 to 819	n/a	no
03-10	H_2/3% H_2O	0.54	0.15	28.4	0.512	0.15	26.9	1053 to 1064	517 to 540 to 517	no
	Dry CH_4	0.499	0.083	14.5	n/a	n/a	n/a	937 to 913	66 to 52 to 83 to 80 to 74 current	no
	Dry odorized NG (93% CH_4)	0.499	0.074	13.0	n/a	n/a	n/a	814 to 678	74 to 47 current	no
03-13	H_2/3% H_2O	0.563	0.2	39.5	0.506	0.19	33.7	1045 to 1059 to 1052	563 @ 200 mA to 558 @150	no
03-14	H_2/3% H_2O	n/a	n/a	n/a	n/a	n/a	n/a	733 fluctuating	n/a	no
03-15	H_2/3% H_2O	0.557	0.075	14.7	0.518	0.08	14.5	947 to 974 fluctuating	550 to 560 fluctuating	no
03-16	H_2/3% H_2O	0.635	0.1	22.3	0.497	0.13	22.7	940 to 936	654 to 478	no
03-18	H_2/3% H_2O	0.521	0.2	36.6	n/a	n/a	n/a	1080 to 1074	521 to 464	no
03-19	H_2/3% H_2O	n/a	n/a	n/a	n/a	n/a	n/a	509 to 564 to 556	n/a	no
03-23	H_2/3% H_2O	0.498	0.224	39.1	0.5	0.21	36.8	1071 to 1075 to 1068	170 to 182 current	no
	Dry CH_4	0.498	0.055	9.6	0.502	0.04	7.0	890 to 869	55 to 58 to 42	no
03-24	H_2/3% H_2O	0.551	0.125	24.2	0.504	0.16	28.3	1054 to 1053	551 to 516 due to thermal cycle	no
03-25	H_2/3% H_2O	n/a	n/a	n/a	n/a	n/a	n/a	927 to 1031 to 347	n/a	no
03-26	H_2/3% H_2O	0.645	0.1	22.6	0.498	0.115	20.1	1095 to 1106	626 @ 100 mA to 544 @ 80 mA	no
	Dry CH_4	0.575	0.01	2.0	0.509	0.011	2.0	853 to 866 in 6 min	575 to 564	no
03-27	H_2/3% H_2O	0.622	0.05	10.9	0.51	0.065	11.6	1034 to 1029	598 to 622	no
03-29	H_2/3% H_2O	0.641	0.04	9.0	0.497	0.05	8.7	107 1 to 1058	641 to 585 to 619 to 590	no
	Dry CH_4	0.53	0.03	5.6	0.514	0.03	5.4	976 to 984	530 to 538	no
03-30	H_2 w/3% H_2O	0.54	0.175	33.2	0.509	0.17	30.4	1080 to 1076	540 @ 175 mA to 539 @ 100 mA	no
	Dry CH_4	0.655	0.025	5.7	0.466	0.025	4.1	854 to 730	655 @ 25 mA to 503 @ 6 mA	no
	58%H_2/22% CO_2/20%H_2O	0.633	0.05	11.1	0.511	0.075	13.4	970-981 to 960-992	633 to 600-630	156-160 mV @ 75 mA

At 700C, the OCV values were relatively stable on H_2. However, the OCVs again usually declined after the cell was switched to hydrocarbon fuel and the OCV decline appeared to correlate with carbon deposition. Declining OCV with time and carbon deposition were less severe at 700°C than at 800°C, allowing operation for longer periods on dry methane fuel. The electrical performance of the cells again tracked the changes in cell OCV.

At 700C, cells operating on H_2 operated for up to 1200 hours. The maximum operation on dry CH_4 was 455 hours – a considerable improvement over the best ~70 hours life obtained at 800C.

Effects of Sulfur Compound Addition

Only cell 03-10 operated on a sulfur-containing full spectrum natural gas at 700°C. Similar to some of the 800°C results, the maximum power density on dry odorized natural gas was similar to the power density obtained when the cell was operating on dry CH_4. However, the addition of sulfur odorant did not prevent an OCV decline in this cell. OCV's as high as 0.937V were obtained on dry CH_4 before a gradual decline set in during the latter half of the test. On switching to odorized natural gas, the rate of the OCV and performance decline increased. The higher hydrocarbon content in natural gas could have contributed to this behavior.

Thick-Electrolyte Cells at 800°C

Tables XIV – XVI summarize the tests performed at 800C on cells with thicker, ~83 µm, electrolytes and thinner, <200 µm anodes. The tables are similar to those presented for "standard" cells. This data was expected to address some of the reliability issues with the standard, thinner-electrolyte cells.

Electrochemical Performance and Carbon Formation

Cell 03-05 and 03-07 were among the best performing cells. The cells operated for 305 and 239 hours and produced maximum power densities of 52.3 and 99.1 mW/cm^2, respectively; on dry CH_4 at 800C with no sulfur compound addition. Carbon deposition was relatively minimal in cell 03-05, but very heavy in cell 03-07. Since both the electrolyte thickness was increased and the anode thickness was decreased, further results will be needed to determine whether improved electrolyte integrity or anode structure are the principal factors responsible for the improvement.

Figure 6 compares the results for cells 03-07 and 03-05. Unlike previous tests, the intermittently measured OCV for cell 03-05 was stable over time at ~980 mV.

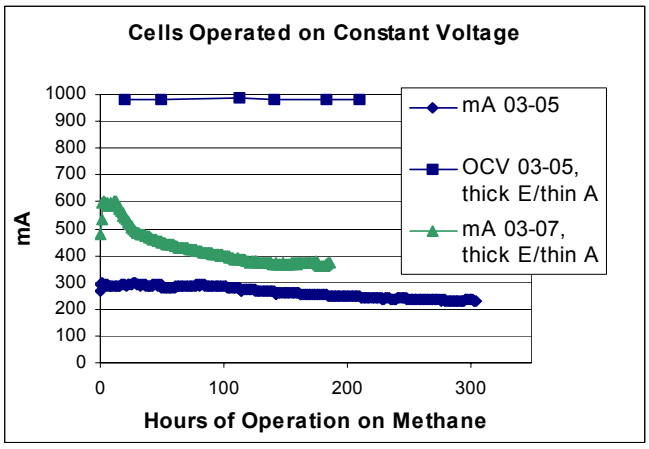

Figure 6: The performance of cells 03-05 and 03-07 on dry methane at 800°C

Table XIV: Objectives and Components for "Thick" Electrolyte Cells at 800°C

[Unless otherwise noted: ~194µm anode impregnated with 20%Cu/10%ceria, ~83 µm electrolyte, ~46 µm LSM, Cu screen/contact lead on anode and Ag screen/contact on cathode. Oxidant is air with 3% H_2O.]

Test #	Objective	Fuel	Component # and Impregnation	Test Station	Anode Seal	Cathode Seal
03-05	Electrochemical performance at constant, 0.5V with programmable electronic load (PEL)	H_2/3% H_2O	SA121002-32	s-4	talc-mica-talc	cement
		Dry CH_4				
03-07	Repeat 03-05 test [0.5V w PEL], anode cemented	H_2/3% H_2O	SA121002-33	s-3	cement	mica
		Dry CH_4				
03-12	Dry CH_4 OCV vs. time	H_2/3% H_2O	SA121002-40	s-4	talc-mica-talc	cement
		Dry CH_4				
		N_2/3% H_2O				

Table XV: Duration and Degradation for "Thick" Electrolyte Cells at 800°C

Test #	Fuel	Operation (Hours)	Carbon	Cu Segregation	Comments
03-05	H_2/3% H_2O	1	minimal; heavier around seal	none visible	
	Dry CH_4	305			
03-07	H_2/3% H_2O	1	heaviest ever (> 1/2")	none visible	Apparent temporary performance improvement from carbon deposit.
	Dry CH_4	239			
03-12	H_2/3% H_2O	1024	none	none visible, anode bright copper	
	Dry CH_4	40			
	N_2/3% H_2O				

Table XVI: Performance for "Thick" Electrolyte Cells at 800°C

Test #	Fuel	Max Operating Voltage	Max Operating Current	Max Operating Power Density	Max Polarization Voltage	Max Polarization Current	Max Polarization Power Density	OCV Change Over Time	Performance Change Over Time	IR
03-05	H_2/3% H_2O	0.93	0.1	32.6	0.5	0.42	73.7	1014 single pt.	930 single pt.	no
	Dry CH_4	0.5	0.298	52.3	n/a	n/a	n/a	980 to 986 to 980	270 to 298 to 230 current	no
03-07	H_2/3% H_2O	0.5	0.948	166.3	n/a	n/a	n/a	n/a	948 current single pt.	no
	Dry CH_4	0.5	0.565	99.1	n/a	n/a	n/a	n/a	565 to 317 current	no
03-12	H_2/3% H_2O	0.557	0.45	87.9	0.498	0.5	87.4	1018 to 1031	545 @ 350mA to 557 @ 450 mA	no
	Dry CH_4	n/a	n/a	n/a	n/a	n/a	n/a	909 to 835	n/a	no
	N_2/3% H_2O	n/a	n/a	n/a	n/a	n/a	n/a	657 to 25	n/a	no

The power density for cell 03-05 was rather stable, whereas the power density for cell 03-07 reached a maximum and then declined. This increase is attributed to improved electrode conductivity caused by the initial production of carbon as discussed in the literature (reference). The differences between the cell performances have different possible interpretations as cited for the standard cell data, but overall, thick-electrolyte cells appear to perform better than the standard thin-electrolyte cells.

However, Cell 03-12, which was an attempt to reproduce cell 03-05 and 03-07 results, did not perform well on dry methane. In this case, the OCV dropped quickly. We believe that a poor seal or another problem with the test may have compromised performance. Attempts to restore performance by returning to operation on hydrogen were not successful. After the test, the anode was bright orange and had little or no carbon. H_2 may have cleaned the electrode, but still left the cell in a compromised condition. XRD indicated that the orange color of the anode is metallic copper and not an unusual copper alloy. The anode also contained cerium oxide, YSZ and no other materials.

Thick-Electrolyte Cells at 700°C

Tables XVII – XIX summarize the tests performed at 700C on cells with thicker, ~83 μm, electrolytes and thinner, <200 μm anodes. The tables are similar to those presented previously.

Electrochemical Performance, Carbon Formation, Sulfur Compound Effects

Test results were consistent with lower power density, less carbon formation, and longer cell life on dry CH4 at lower temperatures.

Cell 03-11 was concluded after 351 hours on dry CH_4 and 34 hours on odorized natural gas (93% CH_4). This was the longest duration obtained with methane fuel. Stable OCV's on the order of 0.9V were obtained on dry CH_4, but the OCV started to decline after switching to odorized natural gas. Changing the anode flow by adding 20 cc/hr of water to hydrogen fuel restored the OCV on H_2 to the 1.029V value observed at the beginning of the test. However, switching back to operation on dry methane produced an unstable and low OCV.

U-Penn style cell 03-28 - tested in a set-up adapted to very small area - had repeated problems with the breaking of the Ag wire contact. The cell only operated on methane for 24 hours. The anode itself was gray with a slightly darker strip near the electrolyte. Carbon deposition otherwise was minimal. Copper segregation was moderate, with the Au paste containing Cu - as indicated by the copper color of the Au paste on the anode surface.

Interaction with the University of Pennsylvania

Interactions with U-Penn enabled some narrowing of the possible causes of excess carbon deposition in the GTI experiments. However, the project scope did not allow elimination of this problem or reaching final conclusions on this question.

The observation by U-Penn that a "standard" GTI cell cut to U-Penn dimensions and tested at U-Penn did not produce excess carbon suggested that GTI could produce a cell that was not itself a source of carbon. This result left the possibilities that

- GTI's larger area cells (2.85 cm^2) are different than a small, 0.33- cm^2-cell. For example, the larger-area GTI cells could have had more electrolyte pinholes or cracked more easily whereas the smaller cell tested at U-Penn might been subject to this.

Table XVII: Objectives and Components for "Thick" Electrolyte Cells at 700°C

[Unless otherwise noted: ~194µm anode impregnated with 20%Cu, 10%ceria, ~83 µm electrolyte, ~46 µm LSM with Cu screen/contact lead on anode side and Ag screen/contact lead on cathode. Oxidant is air with 3% H2O.]

Test #	Objective	Fuel	Component # and Impregnation	Test Station	Anode Seal	Cathode Seal
03-11	Dry CH_4 and N.G. OCV with "steam cleaning" to remove C.	H_2/3% H_2O	SA121002-37	s-1	talc-mica-talc	cement
		Dry CH_4				
		Dry odorized NG (93% CH_4)				
03-17	Dry CH_4 with change in cathode seal.	H_2/3% H_2O	SA121002-41	s-1	talc-mica-talc	Ultra Temp 516
03-28	Small cell (0.33 cm^2) from U-Penn; converted test set-up. Ag wire on cathode side, Au wire on anode, ~600-µm anode, ~80-100-µm electrolyte, LSM	H_2/3% H_2O,	UPEN-01, sequential	s-3	open to air	Ceramabond 552
		dry CH_4				

Table XVIII: Duration and Degradation for "Thick" Electrolyte Cells at 700°C

Test #	Fuel	Operation (Hours)	Carbon	Cu Segregation	Comments
03-11	H_2/3% H_2O	144	minimal; heavier around seal	none visible	
	Dry CH_4	351			
	Dry odorized NG (93% CH_4)	24			
03-17	H_2/3% H_2O	1135	n/a	none visible	Performance was poor due to failure of a relay in the heater. First cell run with Aremco cement on cathode side.
03-28	H_2/3% H_2O,	205	minimal; visible near electrolyte	moderate; gold paste full of Cu	Cell package broke into pieces during removal from the hardware.
	Dry CH_4	24			

Table XIX: Performance for "Thick" Electrolyte Cells at 700°C

Test #	Fuel	Max Operating Voltage	Max Operating Current	Max Operating Power Density	Max Polarization Voltage	Max Polarization Current	Max Polarization Power Density	OCV Change Over Time	Performance Change Over Time	IR
03-11	H_2/3% H_2O	0.632	0.125	27.7	0.477	0.125	20.9	1014 to 1031	570 @50 mA to 530 @ 125 mA	no
	Dry CH_4	n/a	n/a	n/a	n/a	n/a	n/a	900 to 894	n/a	no
	Dry odorized NG (93% CH_4)	n/a	n/a	n/a	n/a	n/a	n/a	893 to 861	n/a	no
03-17	H_2/3% H_2O	0.558	0.275	53.8	0.501	0.32	56.3	724 to 921	505 to 558	no
03-28	H_2/3% H_2O	0.608	0.02	36.8	n/a	n/a	n/a	1078 to 1083	591 @ 20 mA to 562 @ 13 mA	no
	Dry CH_4	0.454	0.005	6.9	n/a	n/a	n/a	757 single pt.	454 to 343	no

- Other factors relating to the larger-area GTI cells could have contributed to excess carbon. Examples include: (1) the possibility of increased effects of low pore size and porosity over a larger area as compared with the more open microstructure of U-Penn cells, (2) increased residence time, (3) absence of small-cell "edge" effects, etc.
- GTI's test procedures increased carbon formation. For example, the GTI cell temperatures could be different than those quoted for other cells because of thermocouple location and furnace dimensions. Or, factors such as time at open circuit, or cell heating and reduction protocols, or fuel utilization might have affected carbon formation.
- GTI's test stand components including seals and contacts could have contributed to carbon formation. In this respect, GTI did rule out impurities in the alumina tubes.

The project ended before the open U-Penn microstructure could be reproduced or U-Penn could test more GTI cells.

GTI's 03-28 test of a U-Penn style cell and other tests involving U-Penn inks were inconclusive in that the U-Penn contacting procedures were not reproduced closely enough to draw meaningful results. Thus, the project did not give direct results on the influence of GTI testing procedures and equipment.

Mechanisms of Direct Utilization of Methane Fuels

The introduction indicated that a direct oxidation mechanism has previously been proposed for utilization of dry methane fuels in the systems investigated here. However, the mechanism is still not well understood. We propose alternative mechanisms below.

Internal Reforming

Technologix Corporation, working with GTI, identified the first mechanistic possibility. An initial step, involving low conversion of methane by internal reforming with adventitious or product steam, is followed by an equilibrium water-gas shift (WGS) reaction and then electrochemical oxidation of H_2. Leaking seals, electrolyte pinholes, fuel gas contamination, or product H_2O from CH_4 oxidation all could provide the trace water vapor needed for this mechanism.

The previously proposed direct oxidation mechanism and this mechanism are listed below:

Mech 1: Complete electrochemical oxidation of CH_4

$$CH_4 + 4O^{=} \rightarrow CO_2 + 2H_2O + 8e^{-} \quad \textbf{(anode)}$$
$$2O_2 + 8e \rightarrow 4O^{=} \quad \textbf{(cathode)}$$
$$CH_4 + 2\,O_2 = CO_2 + 2H_2O$$

Mech 1A: CH_4 reforming with WGS followed by electrochemical oxidation of H_2.

$$CH_4 + 2H_2O \rightarrow CO_2 + 4H_2 \quad \textbf{(anode, reforming with W-S)}$$
$$4H_2 + 4O^{=} \rightarrow 4\,H_2O + 8e \quad \textbf{(anode)}$$
$$2O_2 + 8e \rightarrow 4O^{=} \quad \textbf{(cathode)}$$
$$CH_4 + 2\,O_2 = CO_2 + 2H_2O$$

The reaction products for both Mechanism 1 and 1A are the same, although Mechanism 1A may yield a non-stoichiometric outlet composition under load.

In order to distinguish between these mechanisms, the respective open circuit potentials were predicted for three cases with different gas compositions and temperatures. The gas compositions had progressively lower H_2O and CO_2 levels – so that the last case (Case 3) approached dry CH_4 utilization.

Case 1: **19.61% CH_4 + 80.39% H_2O (4.1:1.0 H_2O/CH_4 ratio) at 800 C**
This composition will not deposit carbon. The OCV for Case 1 is undefined when no CO2 is present in the fuel.

Case 2: **40% CH_4 + 20% CO_2 + 40% H_2O at 700 C**
This composition is located on a carbon deposition boundary (calculations based on graphite) – it will probably not deposit carbon.

Case 3 **1-3% H_2O + 1-3% CO_2 + Balance CH_4 at 800 C**
Carbon deposition is strongly allowed. Some H2O and CO2 was maintained for the OCV to be defined.

Figures 7 - 9 compare the results of OCV calculations assuming low methane conversion and water-shift reaction in equilibrium at all times. At the same time, the OCVs were measured for compositions equal to, or closely approaching, these compositions.

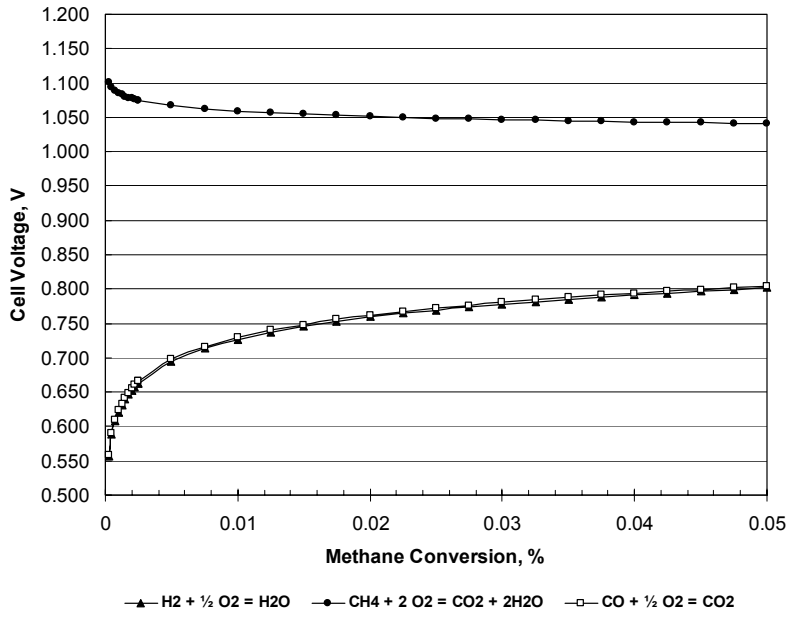

Figure 7. Theoretical OCV for 4.1:1 steam to carbon ratio (19.61% CH_4 + 80.39% H_2O) at 800 C and low CH_4 conversions for the listed mechanisms (water-shift equilibrium assumed) - experimental OCV is 703 mV; theoretical OCV for electrochemical oxidation of H_2 is ~700 mV at 0.6% CH_4 conversion.

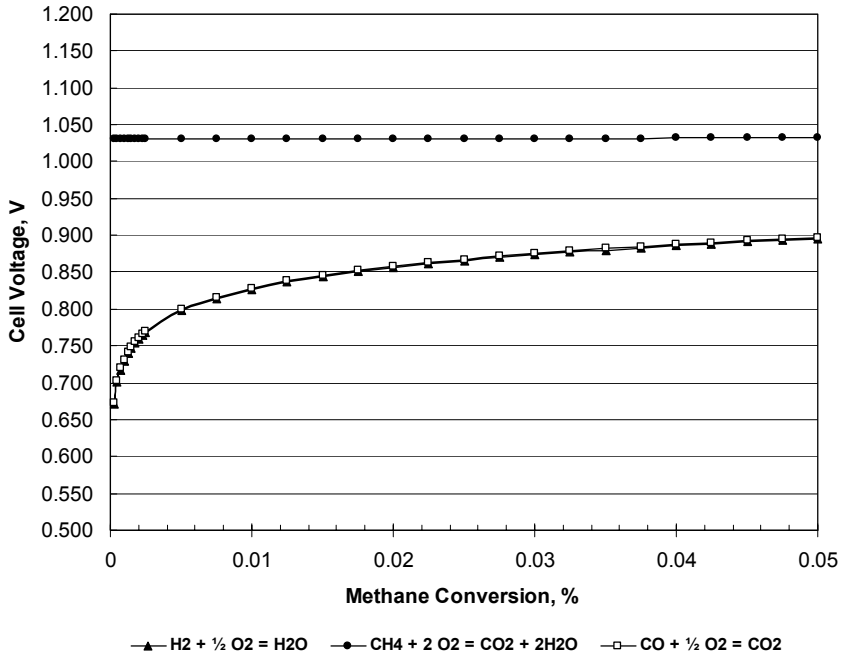

Figure 8. Theoretical OCV for composition 40% CH_4 + 40% H_2O + 20% CO_2 at 700C and low CH_4 conversions for the listed mechanisms (water-shift equilibrium assumed) - experimental OCV is 833 mV; theoretical OCV for electrochemical oxidation of H_2 is ~836 mV at 1.25% CH_4 conversion.

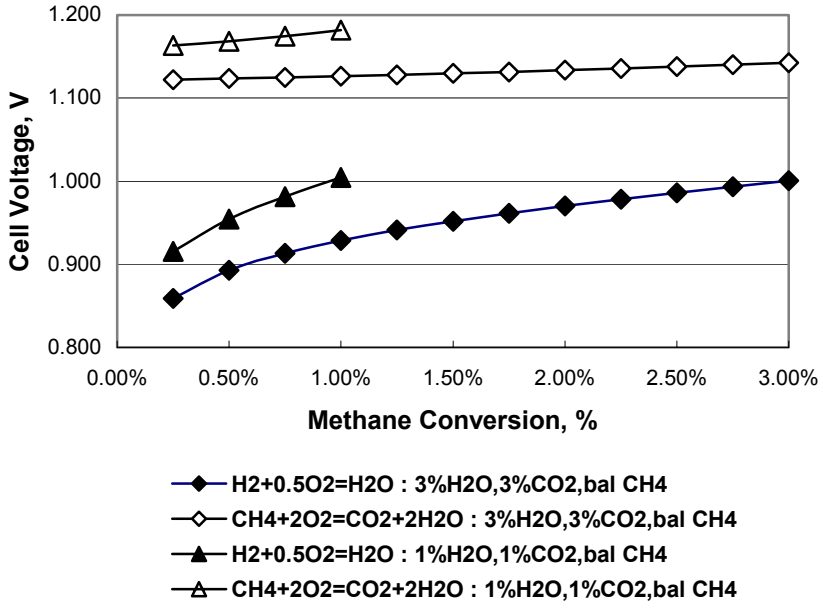

Figure 9: OCV at lower H_2O/CO_2 concentrations for the listed mechanisms (water-shift equilibrium assumed) - the experimental OCV is 980-983 mV; the predicted OCV is 980 mV at 0.75% CH_4 conversion.

Table XX compares the predicted and experimental OCVs for the three cases. In each case, similar conversions of ~1% could be found at which the predicted OCV closely approached the experimental OCV for the reforming mechanism. In contrast, the OCV for direct oxidation deviated strongly from the measured values at all % conversion values up to 5% and higher. Therefore, the possibility of finding any CH_4 conversion for which the direct oxidation OCVs matched was unlikely.

Table XX: Measured and Predicted OCVs for Internal Reforming and Direct Oxidation Mechanisms

Case	Measured OCV (mV)	Predicted OCV for Mechanism 1A (mV)	Predicted OCV for Mechanism 1 (mV)	% CH_4 Conversion
1	703	700	~1100	~1.25%
2	833	836	1030	~0.6%
3	980-983	980	>1100	0.75%

Mechanisms involving the oxidation of CO to CO_2, CH_4 to CO, carbon to CO, and carbon to CO_2 were also evaluated. The first mechanism was excluded because a fast shift reaction under these conditions is expected to preferentially convert CO to H_2. The OCVs predicted for the other mechanisms did not match the measured values.

The analysis identified at least three ways further experimental evidence could distinguish between direct oxidation and internal reforming mechanisms:

- For the same fuel composition, the predicted OCV for direct oxidation is almost independent of temperature, whereas the predicted OCV declines for the internal reforming mechanism.
- OCV should vary directly with p_{CH4}, according to the OCV-defining equation below for direct oxidation. The OCV for internal reforming should only depend on H_2 oxidation.

$$f(E_o) = \exp\left(\frac{8F\left(E_o - E_o^o\right)}{RT}\right) = \left(\frac{p_{O2}^2}{p_{CO2} \cdot p_{H2O}^2}\right) \cdot p_{CH4}$$

1. The H_2/CO contents (~ 0.75% H_2 and ~0.20% CO) at the optimum CH_4 conversion were similar even though temperatures and W-S reaction rates were different. Analysis of the outlet H_2 and CO content would provide further evidence for internal reforming.

Both H_2O and CO_2 are not defined for "dry" CH_4 OCV results reported in the literature. Under these conditions, small variations in H_2O or CO_2 lead to major deviations in computed OCV. The fuel is likely to contain small quantities of H_2O and CO_2 because supplying completely dry fuel is difficult and gas crossover into the anode is probable (lab cell OCVs are reported to be ~60 mV lower than theoretical OCV's). For these reasons, a stable OCV with "dry" CH_4 does not prove direct oxidation.

The stoichiometric proportionality of CH_4 conversion to current as reported in literature (S.Park et al., Figure 5) provides a better rationale for direct CH_4 oxidation, since internal reforming is

less likely to yield stoichiometric proportionality. However, H_2 oxidation under load is also likely to accelerate CH_4 reformation so that the same relationship might still apply with internal reforming.

Another related mechanism could be occurring that also produces an OCV consistent with a H_2/O_2 redox couple. In this mechanism, partial oxidation, $CH_4 + ½\ O_2 \rightarrow 2H_2 + CO$, by air infiltration through perimeter seals and pinholes in the electrolyte is responsible for producing a stable OCV in dry CH_4. The product CO and H_2 would then undergo WGS and H_2 oxidation similar to the reforming mechanism.

The tentative conclusion is that the OCV observed in the GTI cells is likely the result of reaction of dry CH4 with air or water vapor infiltrating the seals and electrolyte.

Reduction of Ceria in the Anode

Another potential direct utilization mechanism is partial oxidation of the CH_4 via reaction with ceria producing carbon deposits and a mixed redox potential. CH_4 would reduce ceria from a +4 oxidation state to a +3 oxidation state, yielding:

$$2CeO_2 + CH_4 \rightarrow Ce_2O_3 + 2H_2 + CO$$

The OCV is a mixed potential that includes the H_2/O_2 and the Ce(IV)/Ce(III) /O_2 redox couples. This mechanism could take place in preference to, or in parallel with, the reforming and partial oxidation mechanisms and is also expected to produce an OCV that is strongly influenced by the H_2/O_2 redox potential.

Out-of-cell Experiments

Three sets of out-of-cell experiments were conducted in which CeO_2 samples were placed in an alumina combustion boat, dried at 120°C, and the boat weighed to the nearest 0.1 mg. The boat was then loaded into a quartz tube and heated to temperature for a designated time under a gas atmosphere flowing at approximately 100 cc/min. After cooling, the boats were reweighed.

In the first set, the samples were heated to 800°C over an 8 hour period, held at 800°C for 16 hours, and then cooled to room temperature over an 8 hour period. The flowing gases used were air, 10% H_2/90% N_2, 100% H_2, and dry 99.97% CH_4. In all cases, the samples lost weight. The weight losses are shown below.

Flowing Gas:	Air	H_2/N_2	H_2	CH_4
% Weight Loss:	0.27%	0.48%	0.49%	1.37%

Heating of the first three samples converted the cerium (IV) oxide from a pale yellow color to a slightly deeper yellow color. The fourth sample, heated under CH_4, turned black. XRD indicated that only CeO_2 was present in the first three samples. The fourth sample contained CeO_2 with a small amount of graphite. The low-resolution XRD mode did not detect any Ce (III) oxide, Ce carbide or Ce nitride in any of the samples.

Visual inspection of the alumina boat for the fourth sample showed gray/black graphite-like deposits on the interior where the ceria sample had been laying but not on those parts of the boat interior and exterior not covered by the ceria. Figure 10 is a photograph of the boat.

Figure 10. Photograph of combustion boat showing graphite deposits on walls covered by ceria during heating in methane.

The deposit had a resistance of <1 Ω indicating its graphitic nature. Graphite deposited in the ceria and on the alumina covered by the ceria but not on the uncovered portion of the boat or on the outside of the boat or on the quartz tubing (not shown).

The second set of experiments weighed ceria (IV) oxide samples heated to different temperatures under flowing CH_4. In the first three tests, the samples were heated to temperature in 4 hours, held at temperature for 16 hours and cooled to room temperature in 4 hours. The samples were heated to 700°C, 750°C and 800°C, respectively. A fourth sample was also heated to 800°C in 4 hours but was held at that temperature for 40 hours before cooling to room temperature in 4 hours. Weighing the samples produced the results below. In all cases the XRD indicated only CeO_2 and graphite were present.

Time @	16 hrs	16 hrs	16 hrs	40 hrs
Temperature	700°C	750°C	800°C	800°C
% Weight Loss:	1.94%	1.76%	1.99%	–4.0% (gain)
% Carbon:	0.48%	0.49%	1.26%	3.63%

A third series of experiments was conducted to determine if the reaction of CH_4 with ceria was indeed limited by the availability of oxygen from the ceria lattice. The boat was heated under CH_4 to a temperature of 700°C, maintained at temperature for for 8, 48, and 100 hours, respectively, and then returned to room temperature at the free fall cooling rate of the furnace. In all cases, carbon deposited within the ceria and in all cases the samples lost weight despite the deposited carbon. The results are as follows:

Time @	8 hrs	48 hrs	100 hrs
Temperature	700°C	700°C	700°C
% Weight Loss:	1.62%	1.88%	1.36%

The ceria used in the 8 hour and 48 hour tests was fresh material from the manufacturer. The as-received material was white in color. The material used for the 100-hour test had been calcined at 700°C in air to burn off the carbon from the previous test. The recycled material was yellow

indicating that it was slightly deficient in oxygen (see first series of tests). Therefore, having been calcined, the 100-hour sample had less oxygen available to react with the CH_4 than did the as-received samples and produced less carbon.

Discussion

In the first experiments, ceria appears to have cracked the CH_4 and deposited graphitic carbon. However, rather than gaining weight, the sample lost weight. This suggests that CH_4 is reducing the cerium (IV) oxide to a sub-stoichiometric oxide and the weight of oxygen lost exceeds the weight of the graphite being deposited. The following is a possible reaction.

$$CeO_2 + \alpha CH_4 \rightarrow CeO_{2-\alpha} + 2\alpha H_2 + \alpha CO;\ 2CO \rightarrow C + CO_2$$

Cerium is known to lose oxygen to form a series of sub-stoichiometric oxides. It is unclear if these are true oxides or simply solid solutions of cerium (III) in cerium (IV) oxide. Knacke, Kubaschewski, and Hesselmann, (1991) list the following range of oxides: CeO, Ce_2O_3, Ce_7O_{12}, Ce_9O_{16}, $Ce_{11}O_{20}$, and CeO_2. The alumina boat experiments clearly indicate that CH_4 is much more effective at reducing Ce(IV) than is H_2.

In the second set of experiments, a limited amount of carbon was deposited at 700° and 750°C, even at extended times at temperature. Carbon deposition appears to cease after about 2% weight loss by ceria, corresponding to $\alpha = 0.1$ in $CeO_{2-\alpha}$.

Carbon deposition appears to stop in the Cu/ceria anode because only a limited amount of oxygen in ceria is available to react with CH_4. If carbon were deposited by a gas phase or catalyzed cracking reaction, carbon deposition should continue at the longer test times.

The first step in the electrochemical oxidation of dry CH_4 on copper/ceria electrodes may be the reaction between CH_4 and ceria to deposit carbon, produce water vapor, and make sub-stoichiometric ceria. This is a chemical reaction that also occurs on open circuit and is responsible for the improvement on electrical conductivity observed in dry CH_4 experiments.

The next step is the electrochemical oxidation of the sub-stoichiometric species back to Ce (IV).

$$CeO_{2-\alpha} + \alpha\ O^{2-} \rightarrow CeO_2 + 4\ \alpha\ e^-$$

Were these the only two reactions occurring at the anode, carbon would build up and foul the electrode blocking further access to the active surface area. For the anode to continue operating for a sustained period of time, carbon must be consumed as fast as it is produced.

Carbon is susceptible to direct electrochemical oxidation and those carbon deposits that form on the electroactive ceria surface may be consumed by electrochemical reaction.

$$C + 2O^{2-} \rightarrow CO_2 + 4\ e^-$$

The steam-carbon reaction also can remove carbon deposits at 800°C.

$$C + H_2O \rightarrow H_2 + CO$$

The steady state composition of the gases within the pore structure of the copper/ceria anode under high electrical loads may be well removed from the range of compositions that deposit carbon at these temperatures, as was surmised by Barnett for the nickel/YSZ anode under high loads. The difference, however, is that under low loads and on open circuit, carbon is deposited by a chemical reaction with ceria, rather than by a catalyzed hydrocarbon cracking reaction and once the ceria is depleted of oxygen, the reaction stops.

At 800C carbon continues to form so that a weight gain results at sufficiently long times. At these temperatures, ceria also appears to catalyze CH_4 cracking.

In the third series of tests, extending the heating time did not increase carbon deposition, again indicating that the reaction between ceria and CH_4 responsible for carbon deposition is limited, most likely by the availability of oxygen from the ceria lattice.

Comparison Between Report Results and the Literature

The results in this project differ in many respects from those reported in the literature. Since the literature results are well supported, GTI believes that explanations will eventually be found for these variations.

As discussed in the report many test configuration, operating condition, and cell design factors - could explain the different results. Test configuration differences involved: the cell support arrangement, the seal materials and arrangement, and the current collection design. Operating condition differences involved: selection and control of cell voltage, implementation and frequency of OCV measurements, and possible differences in fuel utilization and cell temperature. Cell design differences involved factors such as anode thickness, anode porosity and pore structure, distribution of Cu and ceria within the pore structure, cell area, impregnation, possible edge effects, and electrolyte thickness.

Table XXI compares U-Penn and GTI results for future reference.

Table XXI: Comparison of U-Penn and GTI Results

Factor	U-Penn Result	GTI Result
Duration at 800C on dry CH_4	**Lifetime of very small-area, relatively thick electrolyte, Cu/ceria/YSZ cells up to 1000 hours**	**Lifetime of 2.85 cm^2 area cells, usually under 70 hours for standard cells and ~300 hours for thick electrolyte cells. Standard cells have reached 284 hours if sulfur is present.**
Amount of carbon deposition at 800C on dry CH_4.	**Little carbon forms and does not disrupt cell performance.**	**More carbon forms that sometimes improves performance initially by enhancing conductivity, but then causes a sharp decline.**
Effect of current density on carbon formation	**OCV conditions may accelerate carbon deposition.**	**High current density may accelerate carbon formation.**
Nature of the carbon deposit	**Tar-like, conjugated polyolefins that are electrically conductive**	**Graphitic carbon – also electrically conductive.**
Location of the carbon	**Loose film between the electrode and the fuel gas.**	**Often throughout electrode, at the electrolyte/anode interface, and in seal area**
OCV at 700 and 800C.	**0.93 at 800C.**	**792-1033V at 800C. 757 - 976 at 700C.**
OCV variation with time.	**OCV typically not monitored with time.**	**OCV often declines after switching from H_2 to dry CH_4 in a manner that seems to correlate with carbon deposition.**
Sequential impregnation of Ce salts and then Cu salts	**Improves performance modestly, but significantly.**	**No improvement observed.**
Impregnations to reach electrode fill values	**?**	**5**

electrode fill values		
Sulfur compound effect	**Cells tolerate sulfur.**	**Sulfur may inhibit of carbon deposition by CH_4 and extend of cell life. Evidence on the effect of sulfur on power density is mixed.**
Power densities at 800C on CH_4.	**Up to 280 mW/cm^2 with results depending upon pore formers used.**	**Typically, 50 - 115 mW/cm^2 with un-optimized porosity.**
Mechanism of direct utilization of dry CH_4 or natural gas	**Favors direct oxidation by oxygen anions**	**Favors internal reforming or partial oxidation mechanism, including partial oxidation mediated by ceria**
Mechanism of carbon formation with CH_4 at 700 and 800C	**Gas phase cracking.**	**Catalytic surface oxidation by ceria favored at 700C with a contribution from gas phase and/or catalytic cracking starting at 800C.**

CONCLUSIONS

This project provided a basis for improving the direct utilization of as-received methane fuels in SOFC cells with Cu/ceria/YSZ anodes. Conclusions that can be drawn from this preliminary evaluation include:

- Baseline performance data at 700 and 800C suggested that carbon deposition varies strongly with factors as electrolyte integrity, seal integrity, the effect of sulfur compounds, temperature, anode structure, and hardware design.
- Carbon fouling plagued some tests, although not in a consistent manner. Carbon fouling is defined here as the buildup of carbon so as to disrupt the physical structure of the cell. Some cells operated for several hundred hours on dry methane fuel at 800°C without fouling. Others died in less than twenty-four hours.
- The results suggest that the infiltration of oxidant (air) and/or water vapor through the seals or the electrolyte caused partial oxidation or reforming of CH_4 in the interior of the anode, producing carbon monoxide that then deposited carbon in the anode. The more air infiltration, the shorter the time-to-failure. In general, thicker-electrolyte cells appeared to exhibit higher OCVs than thin-electrolyte cells and had longer time-to-failure.
- The addition of sulfur compounds to dry CH_4 appeared to inhibit carbon deposition and extend cell life. Tests conducted with CH_4 odorized with a combination of organic sulfur species and carbonyl sulfide up to 75 ppm total sulfur indicated complete sulfur tolerance. In all experiments, no change in performance was observed. However, when CH_4 containing 100 ppm H_2S was used, the performance decayed in some tests, but not others.
- OCV declines with time often observed after switching fuel from H_2 to dry CH_4 may be due to the formation of carbon bridges across the electrolyte that short the cell or to other effects of carbon deposition such as increased air infiltration through compromised seals. The OCV decline is accompanied by electrochemical performance decline under load.
- Although little work was performed because of the carbon deposition issue, the project showed that the originally proposed Ni interlayer cells could be fabricated and produced power densities, cell life, and sulfur tolerance comparable to cells not containing an interlayer.
- Mechanisms were identified based on internal reforming, partial oxidation, and reduction of ceria in the anode as alternative routes for direct utilization of CH_4. The mechanism involving ceria reduction leads to an interpretation of how and where carbon deposits in comparison with previous explanations involving only gas phase cracking. The mechanism also shows how carbon deposition may be self-limiting at 700-750C.
- This project identified a number of unanticipated problems unique to dry methane cells. Further work is needed on cell fabrication to improve anode microstructure and electrolyte integrity and make stronger cells. Work is needed also to design hardware to prevent air infiltration. The project only evaluated the most restrictive case of using essentially dry fuels. Further work is needed on low-level humidification of the methane fuel to extend cell life.

REFERENCES

1. Singhal, S. C. and Kendall, K.; High Temperature Solid Oxide Fuel Cells: Fundamentals, Design and Applications, Chapter 12, Elsevier, 2003.
2. Tao, S. and J. Irvine, "Synthesis and Characterization of $(La_{0.75}Sr_{0.25})Cr_{0.5}Mn_{0.5}O_{3-\delta}$, a Redox-Stable, Efficient Perovskite Anode for SOFCs," J. Electrochem. Soc., **151**, A252, 2004.
3. Remick, R., T. Osif, and M. Lawson, "Sulfur-Tolerant Anode Materials," Final Report for Contract DE-AC21-86MC23267, September 30, 1988.
4. Singhal, S. C. et al., "Anode Development for Solid Oxide Fuel Cells, Report No. DOE/MC/22046-2371, U.S. Department of Energy, Washington, DC, 1986.
5. Marina, O., N. Canfield, and J. Stevenson, "Thermal, Electrical, and Electrocatalytic Properties of Lanthanum-Doped Strontium Titanate," Solid State Ionics **149**, 21, 2002.
6. Stevenson, J., S. Baxkaran, L. Chick, U.-S. Chou, J. Deibler, M. Khaleel, O. Marina, K. Meinhardt, D. Paxton, L. Pederson, K. Recknagle, S. Simner, V. Sprenkle, K. Weil, Z. Yang, P. Singh, and G. McVay, "Solid Oxide Fuel Cell Development at PNNL," Proceedings of the 8th International Symposium on Solid Oxide Fuel Cells, ed. S.C. Singhal, et al., pp. 31, The Electrochemical Society, Inc., Pennington, NJ, 2003.
7. Pudmich, G., B. Boukamp, M. Gonzalez-Cuenca, W. Jungen, W. Zipprich, and F. Tietz, "Chromite/Titanate Based Perovskites for Application as Anodes in Solid Oxide Fuel Cells," Solid State Ionics, **135**, 433, 2000.
8. Murray, E. P., T. Tsai, and S. A. Barnett, Nature, **400**, 649, 1999.
9. Liu, J. and S. A. Barnett, "Operation of Anode-Supported Solid Oxide Fuel Cells on Methane and Natural Gas," Solid State Ionics, **158**, 11-16, 2003.
10. Park, S., R. Craciun, J. M. Vohs, and R. J. Gorte, "Direct Oxidation of Hydrocarbons in a Solid Oxide Fuel Cell: I. Methane Oxidation," J. Electrochem. Soc., **146**, 3603-3605, 1999.
11. Lu, C., W. L. Worrell, H. Kim, R. J. Gorte, J. M. Vohs, "Characterization of a Cu0.8Ni0.2-CeO2-YSZ Anode-Composite For the Direct Oxidation of Dry Methane", Electrochemical Society, Proceedings Volume 2002-5, 88-96.
12. Kim, H., C. Lu, W. L. Worrell, J. M. Vohs, and R. J. Gorte, "Cu-Ni Cermet Anodes for Direct Oxidation of Methane in Solid-Oxide Fuel Cells", Journal of the Electrochemical Society, 149 (2002) A247-A250.
13. McIntosh, S., J. M. Vohs, and R. J. Gorte, "Effect of Precious-Metal Dopants on SOFC Anodes for Direct Utilization of Hydrocarbons", Electrochemical and Solid State Letters, 6 (2003) A240-A243.
14. Gorte, R. J., S. Park, J. M. Vohs and C. Wang, "Anodes for Direct Oxidation of Dry Hydrocarbons in a Solid-Oxide Fuel Cell," Adv. Mater., **12**, 1465-1469, 2000.
15. Corbin, S. F. and P. S. Apte, "Engineered Porosity via Tape Casting, Lamination and the Percolation of Pyrolyzable Particulates," J. Am. Ceram. Soc., **82**, 1693, 1999.

16. McIntosh, S., J. M. Vohs, and R. J. Gorte, "The Role of Hydrocarbon Deposits in the Enhanced Performance of Direct-Oxidation SOFCs," personal communication.

17. Knacke, Kubaschewski and Hesselmann, eds., Thermochemical Properties of Inorganic Substances, 2nd ed., Springer-Verlag, 1991.

BIBLIOGRAPHY

1. "Oxidation Of Dry And Near-Dry Hydrocarbons At High-Power-Density Anodes," K. Krist, O. Spaldon-Stewart, R. Remick, Gas Technology Institute and J. Jewulski, Technologix Corporation, SECA Core Technology Program Workshop Presentation, Sacramento, CA, February 20, 2003

2. "Options For System Development Using SOFCs," R. Petri, D. Goodwin, K. Krist, E. Ong, J. Pondo, R. Remick, C. Sishtla, O. Spaldon-Stewart, R. Zabransky, 2003 Fuel Cell Seminar Abstracts, p898.

LIST OF ACRONYMS AND ABBREVIATIONS

EDX	Energy Dispersive X-ray spectroscopy
GC	Gas Chromatography
GTI	Gas Technology Insitute
IR	Internal Resistance
LSM	Lanthanum Strontium Manganite
MSRI	Material and Systems Research, Inc.
NG	Natural Gas
NWU	Northwestern University
OCV	Open Circuit Voltage
PEL	Programmable Electronic Load
PMMA	Poly Methyl Methacrylate
SECA	Solid State Energy Conversion Alliance
SEM	Scanning Electron Microscope
SOFC	Solid Oxide Fuel Cell
WGS	Water-Gas Shift (reaction)
XRD	X-Ray Diffraction spectroscopy
YSZ	Yttria Stabilized Zirconia